RICE UNIVERSITY

STATIC MAGNETIC PROPERTIES OF DC BIASED RF SPUTTERED GdFe AMORPHOUS FILMS

by

Robert Zwingman

A THESIS SUBMITTED
IN PARTIAL FULFILLMENT OF THE
REQUIREMENTS FOR THE DEGREE OF

DOCTOR OF PHILOSOPHY

Thesis Director's Signature

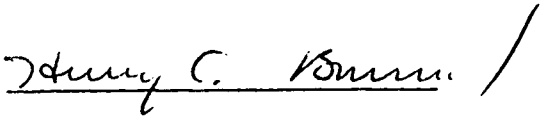

Houston, Texas

April 1976

ACKNOWLEDGEMENTS

I would like to thank my advisor, Dr. Henry C. Bourne, Jr., for his continual constructive advice throughout my graduate career and, in particular, during the writing of this thesis. I would also like to thank Dr. William L. Wilson, Jr., not only for being a great friend, but also for his enthusiasm, advice and sound technical ideas.

I would also like to thank Dr. Pamela J. Sperry for her unlimited patience and encouragement throughout my stay at Rice.

I would like to acknowledge Mr. and Mrs. Clarence J. Zwingman, my parents, whose patience and understanding have made more than just this thesis possible.

TABLE OF CONTENTS

INTRODUCTION:

The static magnetic properties of d.c. bias sputtered gadolinium-iron thin films are reported and the origins of some of these properties are found. The room temperature magnetic properties relevant to magnetic bubble domain materials are given the major considerations in this work. However, it should be noted that the objective of this thesis is not to design or perfect a magnetic bubble material but, first, to find the magnetic properties and their origins for GdFe bias sputtered films and, second, to evaluate these films for bubble material purposes.

The remainder of this chapter covers some of the basic concepts of bubble domains and bubble domain devices. These concepts are presented to introduce the important static magnetic properties of bubble materials and what are reasonable values for practical bubble materials.

The chapter on amorphous magnetic materials draws on the basic concepts discussed in the introductory chapter. This chapter gives a literature review of the amorphous magnetic materials which have properties that are important in considering an amorphous material for a bubble material.

The experimental techniques are described in Chapter III.

The results and discussion section gives the data observed, the magnetic properties deduced from the data and a comparison of film properties with those properties found by other researchers for both GdFe and GdCo films. The magnetic properties investigated are: magnetization, wall energy, anisotropy, exchange stiffness and coercivity. Other properties investigated are: film stress, thermal contraction effects, argon inclusions, bias effects, resistivity and ordering effects.

The concluding chapter is a summary of the properties found and an evaluation of bias sputtered GdFe films for bubble material purposes.

Material Considerations:

The optimum magnetic properties of a bubble material must be known in order to evaluate GdFe films as possible bubble materials. Bubble domain devices determine the specifications for a bubble device material. The concept of a magnetic bubble and a bubble domain propagation circuit are briefly covered to show what are optimum material specifications and how they are obtained.

Consider a platelet of magnetic material that has the property that it is energetically favorable for the magnetization to lie normal to the surface of the platelet. For certain combinations of the magnetization, anisotropy, coercivity and exchange stiffness the platelet will demagnetize itself into a multidomain structure. Such a structure is shown in figure 1a. The domains are separated by magnetic domain walls. A common magnetic parameter used to characterize a domain wall is the wall energy, σ_w. The wall energy in a uniaxial bubble material with simple Bloch walls is a function, $\sigma_w = 4\sqrt{AK_u}$, only of the anisotropy energy constant, K_u, and the exchange stiffness constant, A.

If the magnetic platelet in figure 1a is subjected to a normal external magnetic field, H_{bias}, the domains aligned parallel to the field will expand at the expense of the domains aligned antiparallel to the applied field. As the field intensity is further increased some of these stripes coalesce into circular bubble domains. See figure 1b. This field value is called the stripe to bubble transition field. Increasing the field further reduces the diameter of the bubble until the bubble eventually collapses.

If a magnetic bubble is subjected to a lateral gradient in the bias field the bubble will usually experience a net force close to the direction

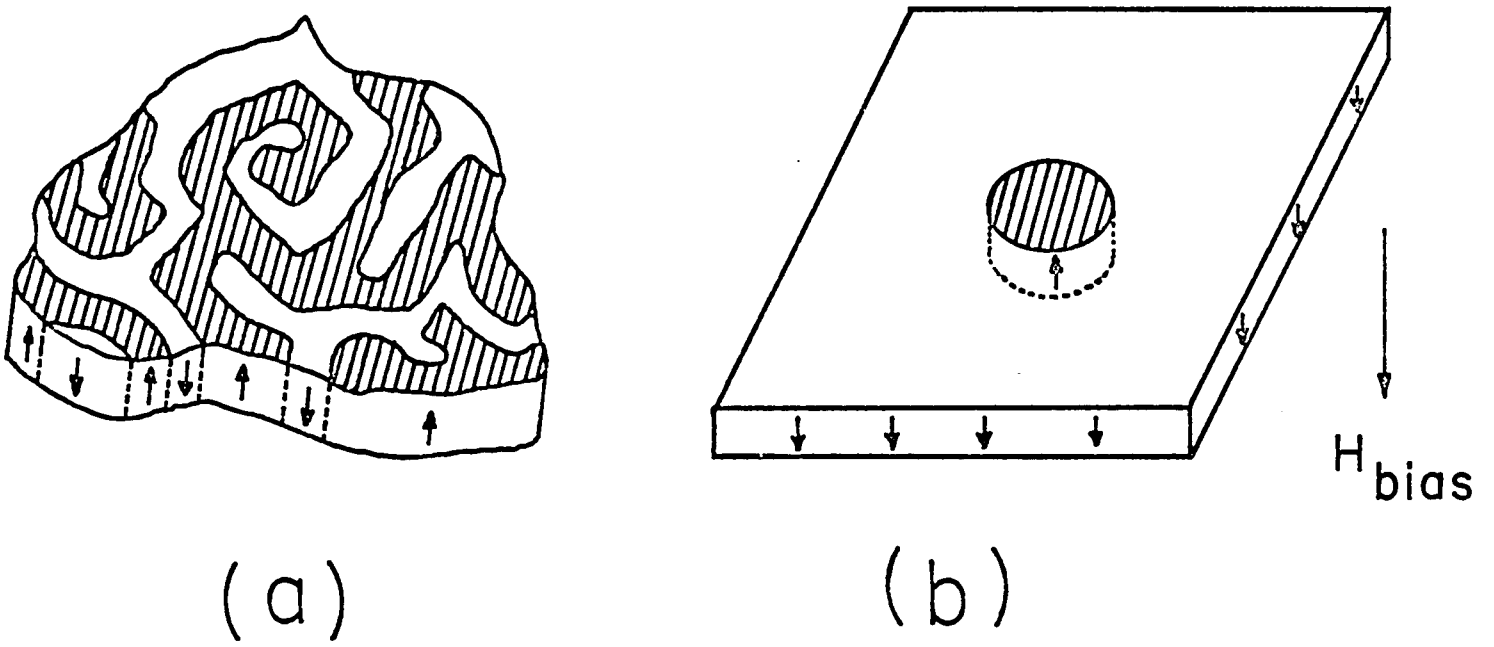

Figure 1: (a) Bubble material platelet with no applied bias. (b) A magnetic bubble domain.

of lower bias [1]. If the domain wall coercivity is low enough the bubble will undergo translation. And, needless to say, if there is a local minimum in the bias field the bubble will come to rest at the location of this field minimum.

A common propagation circuit using magnetic bubbles is called a T-I bar circuit. A segment of this circuit is shown in figure 2. For this circuit, the bubble material is overcoated with a silicon dioxide layer. The SiO_2 layer is then coated with permalloy, NiFe, layer. Permalloy is a high magnetization, magnetically soft material. The permalloy overlay is etched to form the T-I bar pattern.

In addition to the applied normal d.c. bias field, an in-plane rotating magnetic field is applied to the whole device. The in-plane field rotates the magnetization direction of the permalloy elements. The stray fields produced at the end of the T and I bars depend upon the direction of magnetization and the overall shape of the elements. In the bubble material the stray fields have a component of magnetic field normal to the platelet surface. Thus the effective bias field is locally altered to produce maximums and minimums. Contour maps of the magnetic potential for a T-I bar device and other overlay circuits can be found in Magnetic Bubbles by A. H. Bobeck and E. Della Torre [G3]. The local minimums in the bias field will propagate along the T-I bar structure if the magnetization direction of the overlay elements is rotated. If a bubble is placed at one of these field minimums it also will propagate. Thus we have a way of propagating a binary digit of information.

The most important bubble material requirements for a device are: 1) there must be enough normal anisotropy to keep the magnetization in the normal direction even in an environment of stray fields and applied

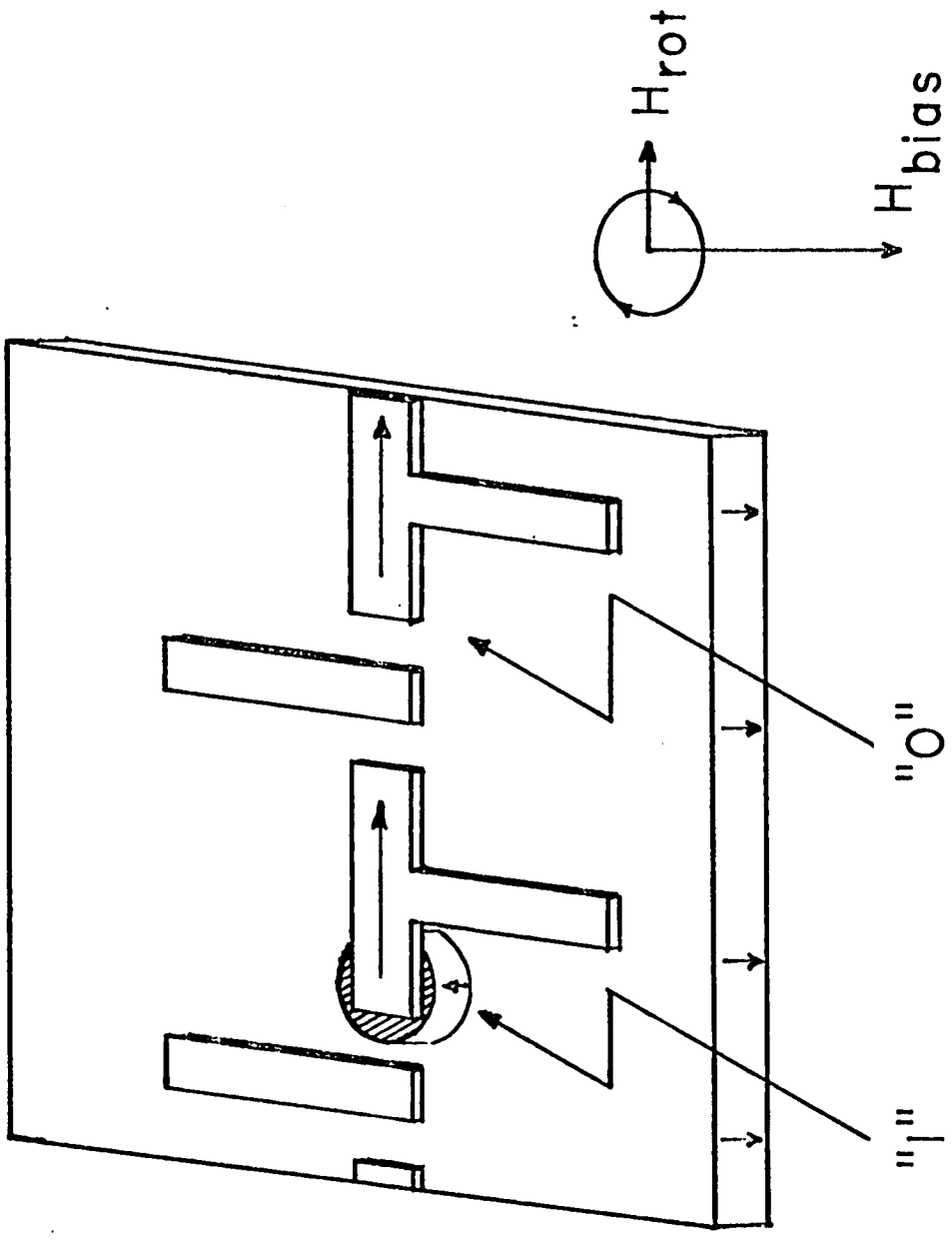

Figure 2: Segment of a T-I bar circuit.

in-plane fields. 2) The material must have a low domain wall motion coercivity to ensure that the bubbles will propagate. 3) The combination of magnetization, anisotropy, coercivity and exchange stiffness and the platelet thickness must be such that there is a bias range where stable bubbles can exist.

Besides these important requirements, other constraints are set because of practical considerations. Such considerations are: 1) Bubble devices must be competitive with existing memory technologies. This imposes bit density, access times, power consumption, and production cost limitations. 2) Low magnetization bubble materials are desired because they require lower in-plane rotating fields and are thus easier to operate. 3) Bubble size must be compatable with the overlay pattern size. 4) Bubble domain devices must be inexpensive to operate.

The above considerations dictate the magnetic parameters for a bubble material. The parameters, given in Table I, are the desired specifications for a 10^7bit/in^2 T-I bar device. The equations relating some of these parameters are:

$$H_k = 2K_u/M_s$$

$$\sigma_w = 4\sqrt{AK_u}$$

$$\ell = \sigma_w/(4\pi M_s^2)$$

where K_u is the uniaxial anisotropy constant and σ_w is the magnetic domain wall energy. ℓ is the characteristic length.

TABLE I:

STATIC MATERIAL SPECIFICATIONS

10^7 BIT/IN^2 T-I BAR DEVICE

BUBBLE DIAMETER	$d \sim 2$ um
STRIPE PERIOD	$P_o \sim 4$ um
MAGNETIZATION	$4\pi M_s \sim 200 - 400$ G
ANISOTROPY FIELD	$H_k \sim 2 - 4 \cdot (4\pi M_s)$
CHARACTERISTIC LENGTH	$L \sim .25$ um
EXCHANGE CONSTANT	$A \sim 2 \times 10^{-7}$ erg/cm
COERCIVITY	$H_c < .005(4\pi M_s)$

CHAPTER II: AMORPHOUS MAGNETIC BUBBLE MATERIALS

In 1967 A. H. Bobeck published in the Bell Systems Technical Journal a paper entitled, "Properties and Device Applications of Magnetic Domains in Orthoferrites" [2]. In this article a magnetic bubble domain device was used for a digital storage element. The bubble materials used were rare-earth orthoferrite crystals. Since this original work on bubble devices there has been an extensive search for new and better bubble materials. Industry, at present, is using rare-earth garnet materials as the bubble material for their devices.

In 1972 Orehotsky and Schroeder co-evaporated gadolinium-iron films onto substrates held at 77°K [3]. They found five very important properties of these films. First, the films were amorphous; no crystallinity could be observed even at room temperature. Second, films of any composition could be made not just the compositions corresponding to the crystalline phases of bulk GdFe. Third, the magnetization varied smoothly with composition. See figure 3. Note the scatter in the magnetization data of these evaporated films. Fourth, the iron moments coupled antiferromagnetically to the gadolinium moments; thus there is a room temperature composition which has no net magnetization. Such a composition is called a compensation composition. And finally, the magnetization could not be pulled in-plane for the low magnetization compositions. The easy anisotropy axis was suspected to lie normal to the film surfaces. An isotropic in-plane stress was suggested as the cause of the anisotropy.

In 1973, Chaudhari, Cuomo and Gambino realized that a rare-earth transition metal alloy like GdFe may have possibilities as a bubble material [4]. Chaudhari, et. al. deposited GdCo and GdFe films by bias sputtering and observed stripe and bubble domains in these films. Since

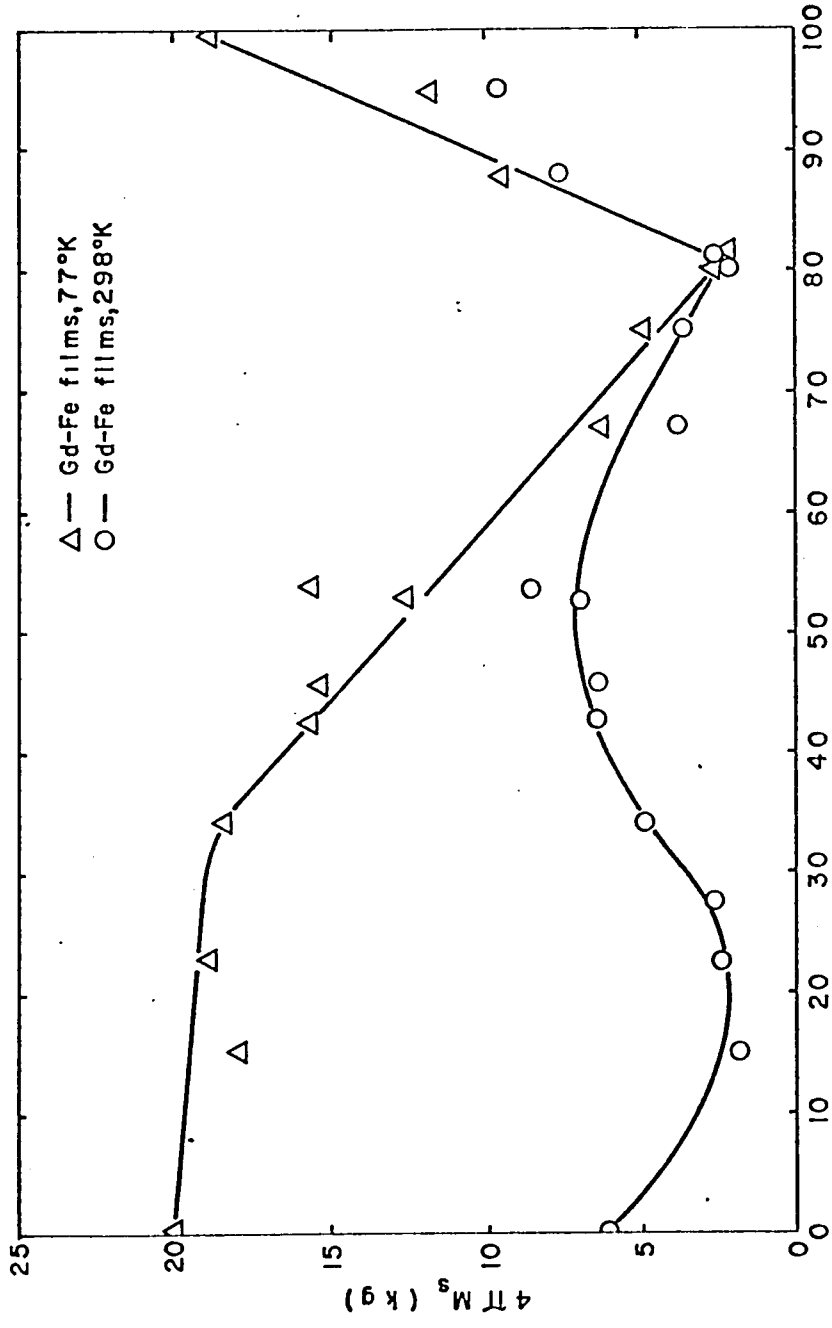

Figure 3: Magnetization dependence on composition from Orehotsky and Schroeder [3].

this initial work on amorphous materials, extensive research has been performed on GdCo films for magnetic materials characterization purposes [5,6,7,8,9,10] and for device purposes [11,12,13]. The magnetization versus composition data for bias sputtered GdCo films reported by Chaudhari, et. al. are shown in figure 4; again note the scatter in the magnetization data.

Cobalt moment ordering has been postulated as the anisotropy mechanism in sputtered GdCo films [5,14,15,16]. Cronemeyer [7] suggested ordered cobalt layering effects as the ordering mechanism. Hasegawa, et. al. [14] and Gambino, et. al. [15] suggest transition metal ordering from ion radiation studies on anisotropy and coercivity. Anisotropy induced by an external stress has been ruled out because a multidomain structure can be observed in films which have been removed from the substrates [4].

R. Hasegawa calculated an exchange constant, A_{gdco}, of $6x10^{-7}$erg/cm for bias sputtered $Gd_{1-x}Co_x$ films with x=.78 [6]. D. C. Cronemeyer [5] reports anisotropy energies of $1\text{-}5x10^5$erg/cc while Bourne, et. al. [7] report $10^4\text{-}10^7$erg/cc for bias sputtered $Gd_{1-x}Co_x$ films with x≈.8. The anisotropy energy data of Cronemeyer and Bourne, et. al. are shown in figures 5a and 5b respectively. An anisotropy of $K_u>10^5$erg/cc requires a $4\pi M_s>1000G$ to produce a bubble size of about 2um. $4\pi M_s>1000G$ is considered too large for a practical bubble domain device material.

Ternary elements have been added to GdCo films to lower both the exchange constant and anisotropy energies. GdCo ternary alloy amorphous bubble films have been an extensive area of investigation [17,18,19,20]. One of the reasons ternary elements were added to GdCo and not to GdFe is that GdCo has a higher polar Kerr rotation than GdFe films.

The polar Kerr effect is used to observe the domain structures of

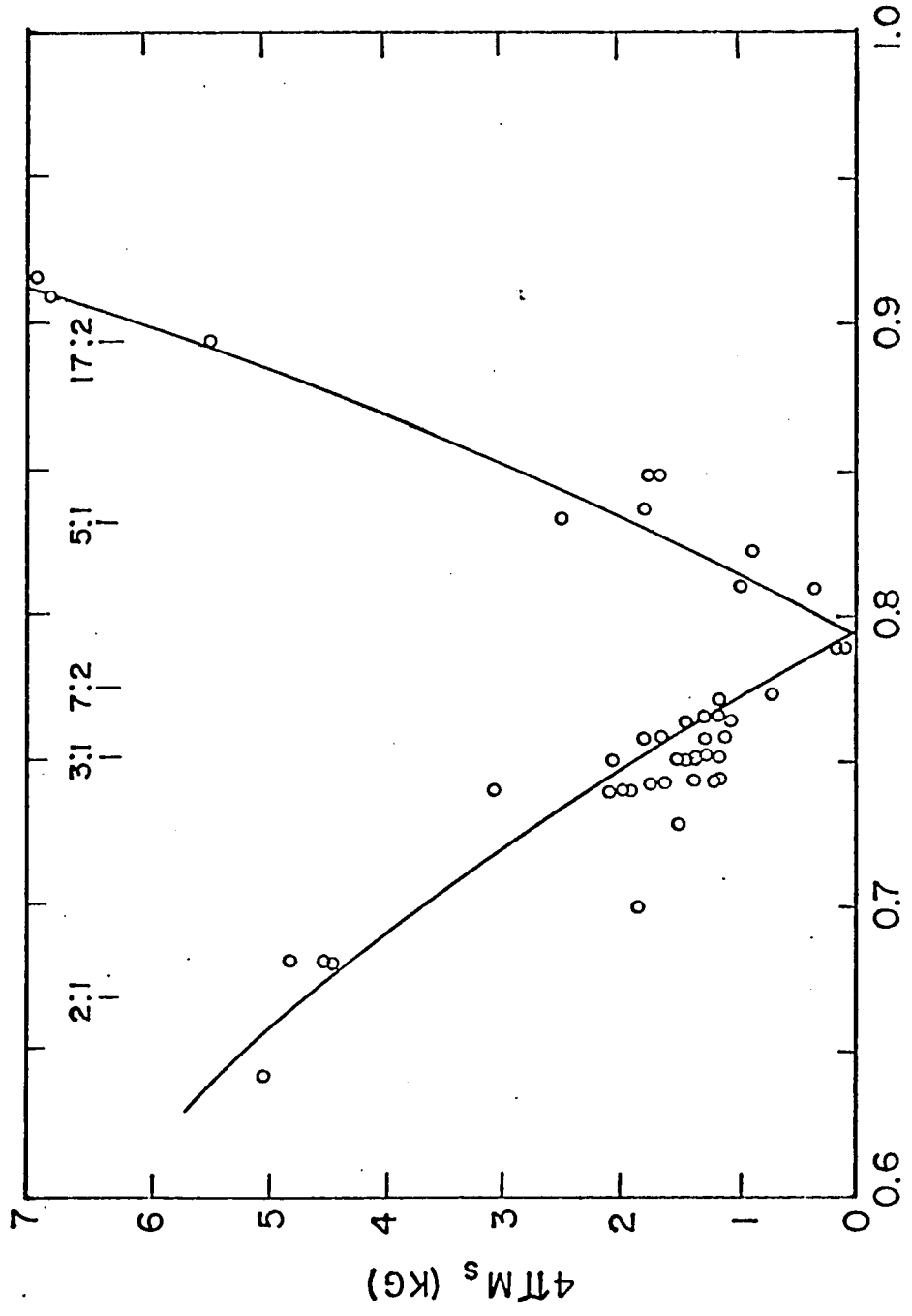

Figure 4: Magnetization dependence on composition for sputtered GdCo films, after Chaudhari, et. al. [21].

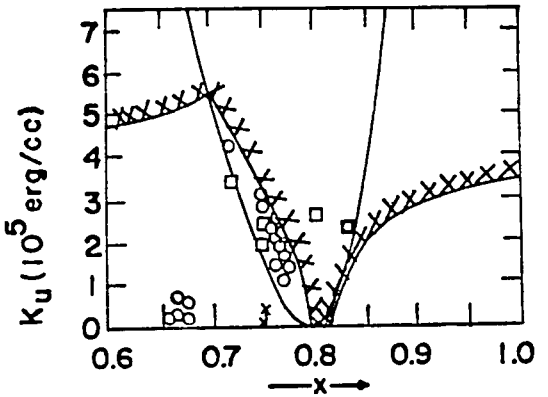

Figure 5(a): The anisotropy energy, K_u, versus composition. Measurement borders of K_u at 9.045GHz are cross-hatched. $K_u=2\pi M_s$ bubble stability limit is also shown. From Cronemeyer [5].

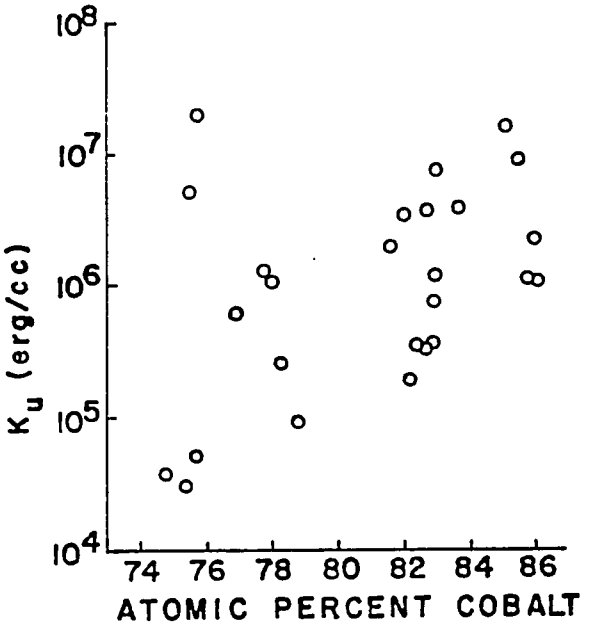

Figure 5(b): Anisotropy dependence on composition for bias sputtered GdCo amorphous films, after Bourne, et. al. [7].

GdCo and GdFe films. GdCo has a polar Kerr rotation of about 15 minutes [21] while GdFe is much smaller, on the order of 5 minutes or less. Even with 15 minutes Kerr rotation the GdCo domains produce poor contrast. GdFe films have about a tenth of the domain contrast since the Kerr contrast is, to first order, proportional to the square of the Kerr rotation angle.

Kobayashi, Imamura and Mimura reported on the static properties of sputtered GdFe films in 1974 [22]. These films were deposited by sputtering onto <111> oriented silicon single crystal substrates. Anisotropy energies of about $2x10^5$erg/cc are reported and stripe widths varying from 4um to .5um for films with $4\pi M_s$ of 200G to 2500G respectively. The stripe widths observed by Kobayashi, et. al. for GdFe and by Hasegawa for GdCo films are shown in figure 6. Note that the stripe widths of the sputtered GdFe films are less than the stripe widths of the bias sputtered GdCo films of similar magnetization. However, the anisotropy energies of these GdCo and GdFe films are about the same. This indicates that the exchange constant, A_{gdfe}, of the GdFe sputtered films is less than the $6x10^{-7}$erg/cc calculated by Hasegawa for bias sputtered GdCo films. A rough estimate of A_{gdfe} is about one-half to one-fourth of A_{gdco} because the stripe widths of GdFe are about a half of the stripe widths of GdCo. See figure 6.

Imamura, et. al. also reported that the angle of the sputter deposition determines the anisotropy axis [23]. Anisotropy axis dependence on the deposition angle is common to evaporated magnetic films [24]; the resultant anisotropy is attributed to long range structural growths. In the same publication, Imamura, et. al. also report that the anisotropy energy, K_u, increases with magnetization to $4\pi M_s$=1000G then K_u slowly decreases with magnetization. This is shown in figure 7. An increasing anisotropy with

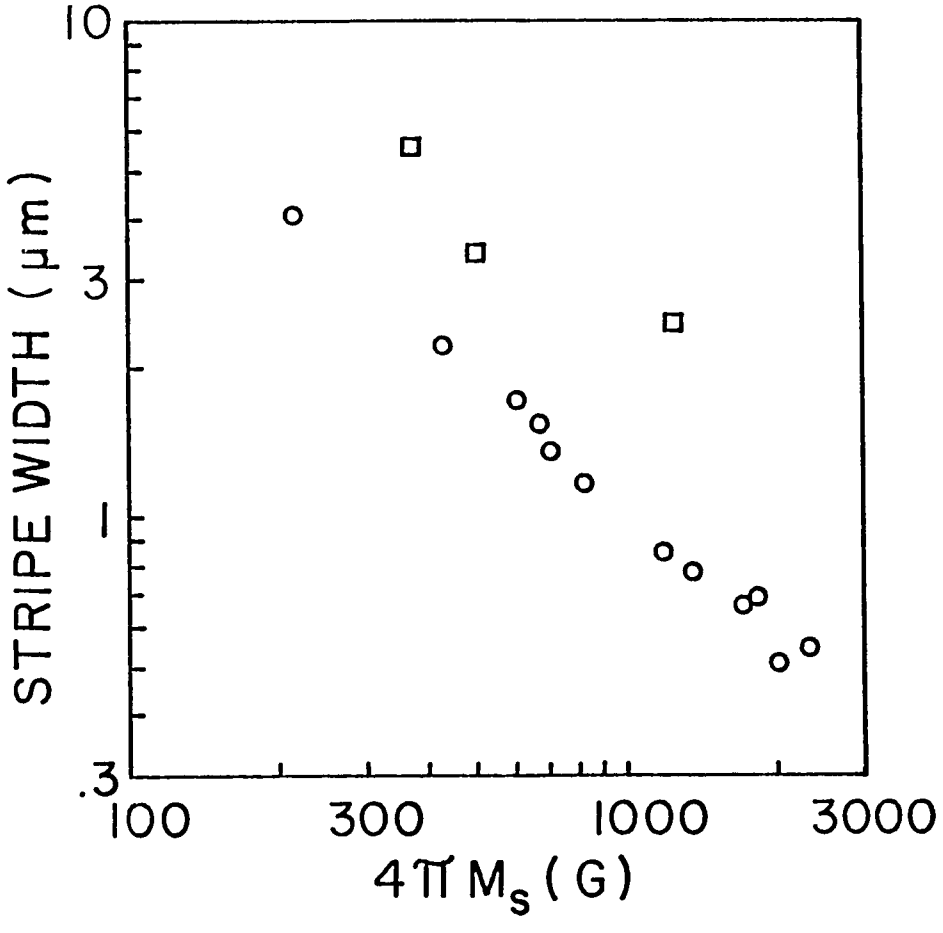

Figure 6: Stripe width dependence on magnetization for GdCo films, squares, from Hasegawa [6]; stripe width data for GdFe films from Kobayashi, et. al. [22].

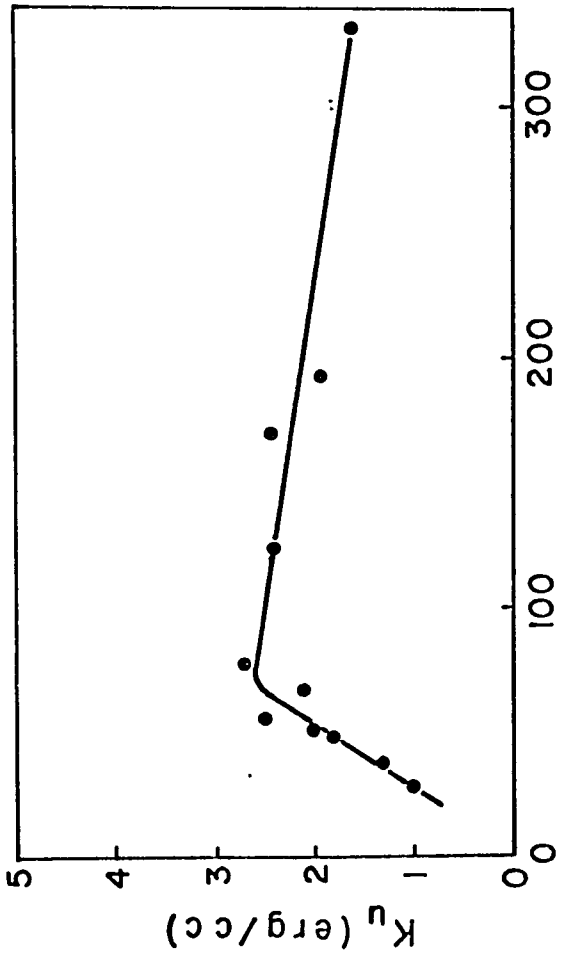

Figure 7: Perpendicular uniaxial anisotropy constant, K_u, dependence on saturation magnetization, M_s, from Imamura, et. al. [23].

magnetization is also observed for sputtered GdCo films with compositions near the compensation composition [5].

Mimura, et. al. [25] reported on the coercivity properties and the preparation techniques of the sputtered GdFe films that were characterized by Kobayashi, et. al. [22] and by Imamura, et. al. [23,26]. The GdFe sputtered films of Kobayashi, Imamura and Mimura were made by co-sputtering from an iron target which supported gadolinium disks. GdFe films were deposited without an applied bias at 130 microns argon pressure. The target to substrate separation was 35mm. Water cooling of both the target and the substrate was used during the deposition. A 400Å/min deposition rate was realized from the 80mm diameter target with 220 watts of rf power delivered to the oscillator. Typical film thicknesses were 1.2um. Their vacuum system was evacuated to 2×10^{-7}torr before bleeding in argon gas. The film composition was adjusted by only varying the number of gadolinium disks supported by the iron target.

The magnetization versus composition data of Imamura, et. al. [23] is shown in figure 8. The room temperature compensation composition is about 26 atm % Gd. The slope of the magnetization versus composition curve is about 400G/atm% for films near the compensation composition.

There are a few papers on evaporated GdFe films besides the initial work published by Orehotsky and Schroeder. Heiman, et. al. [16] and Lee and Heiman [27] report on the anisotropy and magnetization properties respectively of GdFe co-evaporated films. They found that the easy anisotropy axis is dependent upon the deposition angle, similar to that found for sputtered GdFe films. This suggests a structure dependence of anisotropy can be induced by evaporation or sputtering. From magnetization and Curie temperature data of evaporated [27] and information about the

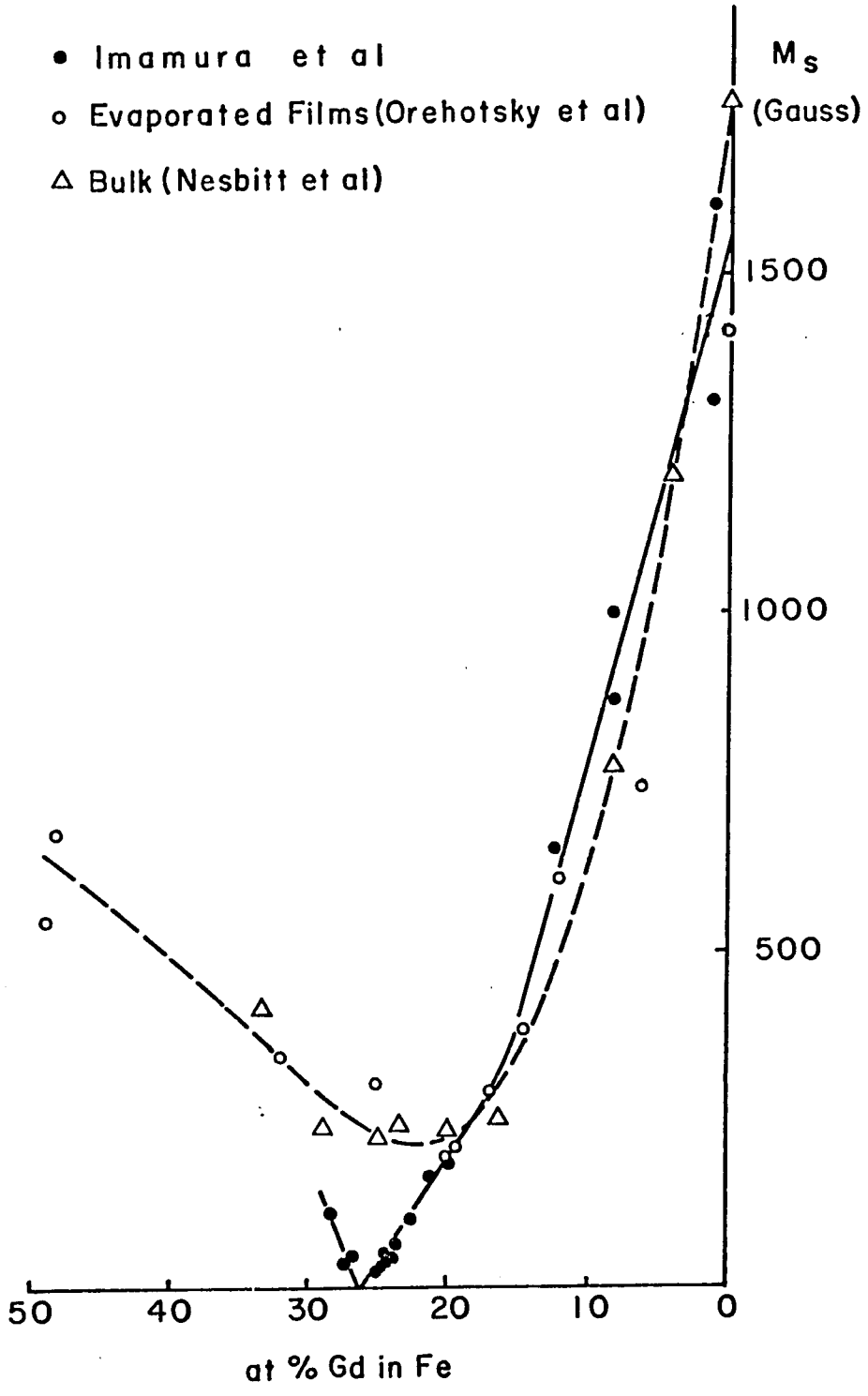

Figure 8: Room temperature saturation magnetization on composition for GdFe alloys prepared by different techniques, from Imamura, et. al. [23].

number of nearest neighbor atoms and their spacing in GdFe amorphous films [28], Lee and Heiman concluded that in GdFe amorphous evaporated films 1) the transition metal moments at 4.2°K are higher than in the equivalent crystalline compounds, 2) the rare-earth magnetic moments at 4.2°K are near their crystalline values and 3) all of the exchange interactions are reduced. Heiman, et. al. [16] postulate, instead of ordering as the cause of anisotropy in evaporated rare-earth transition metal amorphous alloys, a pseudo-crystalline coordination may occur possessing perhaps a preferential orientation or a longer range of coherence along the growth axis than in the directions perpenducular to it. This type of structural growth would be hard to prove for these alloys since there are no crystallites larger than about 20Å to 25Å.

The magnetic properties of evaporated GdFe films have recently been reported by R. C. Taylor [29]. In his work, 5000Å thick films were evaporated into glass substrates held at room temperature. Films were deposited at 10Å/sec from dual electron-beam sources. The films were found to have a room temperature compensation composition of about 26 atm% Gd and a $\Delta 4\pi M_s/\Delta x$=500G/atm% at the compensation composition. Taylor found that the iron and gadolinium moments for his films were very close to the moments observed in the pure bulk elements which are higher than the moments observed in the crystalline GdFe alloys. Anisotropy energies of $2\text{-}4\times10^5$erg/cc and stripe periods slightly larger than those observed by Kobayashi, et. al. are reported. Taylor concludes that the anisotropy is strongly influenced by pseudo-crystalline structural growths of longer range ordering than pair ordering but concedes that pair ordering might contribute to the anisotropy. The magnetization data for the evaporated films of Taylor [29] are shown in figure 9.

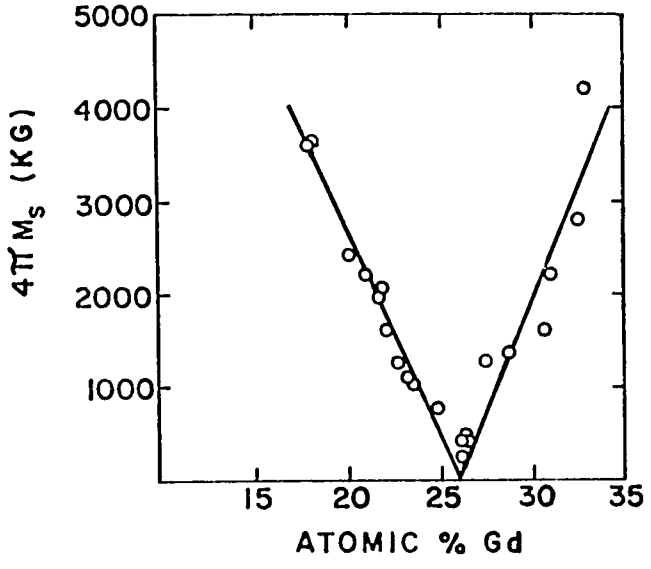

Figure 9: Room temperature saturation magnetization as a function of composition for evaporated GdFe films from Taylor [29].

From the data of Kobayashi, et. al. and from the data of Taylor, a lower exchange constant is expected for GdFe films than GdCo films. Thus sputtered GdFe films may be a better bubble material than sputtered GdCo films if the anisotropy mechanism can be found and, more important, the anisotropy can be adjusted to any desired value. Bias sputtering is known to be a way of affecting the wall energy of GdCo films [4]. For this thesis, GdFe bias sputtered films are prepared and investigated to try to determine if bias sputtering can be used as an effective means of controlling either the anisotropy or the wall energy of the films.

CHAPTER III: EXPERIMENTAL TECHNIQUES AND CONSIDERATIONS

Gadolinium-iron films were prepared by d.c. biased rf sputtering, from an iron target supporting gadolinium disks, see figure 10. The iron target used was made of Armco Iron [30] and has the impurity limits shown in Table II. The solid iron target was 3/8 inches thick and 2.875 inches in diameter. The iron target was mounted on a water-cooled brass post. The gadolinium disks were a quarter inch in diameter and less than 50 mils thick. Their impurity limits are also shown in Table II. Corning 0211 microsheet was used for the substrates because of its "practically flawless, firepolished surface" [31]. The substrates were 15.9mm square by .7mm thick and were held by silicon grease to the substrate holder. Electrical contact was made from the holder to the glass by small conductive copper paint drops placed at the corner of the substrates. The d.c. substrate bias voltage was applied by a regulated voltage supply and was set between 0 and -160vdc. The film deposition started with the opening of a shutter. The bias was not effective until the films were thick enough to be conductive because the substrate bias was d.c. and the substrates were not premetalized. After about five minutes of deposition the d.c. voltage supply started to draw higher currents than when the shutter was just opened. The current increased from about 20ma to about 40ma. This indicates that the bias was not effective for the first five minutes but was effective for the rest of the deposition.

The substrate holder was screwed onto a water-cooled copper fixture. The substrate holder was located 5cm above the target surface. A d.c. magnetic field, used to enhance the plasma at the low pressures, was 112oe at the plasma center and 108oe at the substrate sites. The magnetic field was generated by a water-cooled copper tube coil (1/60 ohm, .59oe/amp)

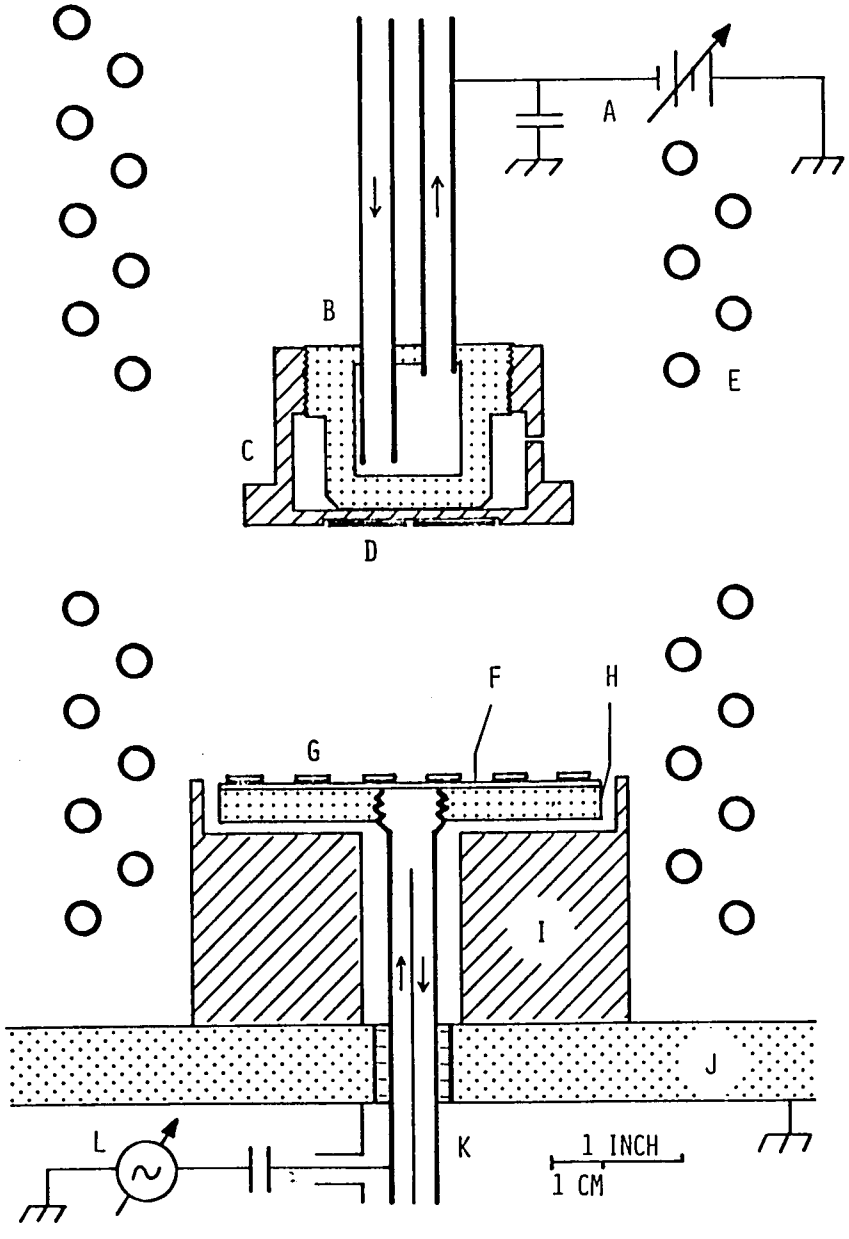

Figure 10: Sputtering system used: A) DC bias is applied, B) the water cooled substrate holder, C) the substrate holder can be easily removed, D) the substrates, E) the DC magnetic field, F) the target assembly, G) gadolinium disks, H) solid iron target plate, I) grounding shield, J) base plate of vacuum system, K) water cooling for target, L) RF supply. courtesy of Ron Goldfarb.

TABLE II:

IRON* (guaranted 99.84%)

Impurity	Typical (%)	Maximum Ladle Analysis(%)		Maximum Sheet And Strip Analysis(%)	
Cu		.15		.18	
S	.025	.030	Total .10	.05	Total .18
C	.015				
Mn	.028				
P	.005	.010			
Si	.003				

Resistivity= 10.7uΩ-cm

GADOLINIUM[+]

Impurity	Typical(%)[++]
Y	.020
Ca	.050
Mg	.005
Si	.001
Fe	.005
Dy	<.005
Sm	.010
Eu	<.005
Total	<.101

Metal produced from 99.9% grade oxides

*Corey Metals, Stock List and Reference Book (undated)

[+]Research Chemicals, Rare Earth Product Catalogue (9/1/74)

[++]The typical analysis is not defined; it could be the final cast ingot, the pre-cast metal, or the oxide from which it was made.

surrounding the target and the substrate holder.

The target self-bias was usually set at -580vdc. The target self-bias could be controlled to about 5% of the desired setting. At -580vdc the target received about 40 watts of power. The oscillator plate voltage and current were nominally 1kvdc and about 55ma. An oscillator efficiency of about 70% is assumed.

The target composition was changed by varying the number of gadolinium disks on the target while the film composition was changed by varying 1) the number of Gd target disks, 2) substrate bias voltage, 3) pressure, and 4) the target self bias voltage.

The vacuum system was evacuated to 5×10^{-7}torr before prepurified argon was leaked into the sputtering system. The argon flow was then adjusted to give a desired pressure. The pressure was monitored by a thermocouple gauge; no automatic pressure controller was used. The pressure reading before and after sputtering varied as much as 10%. Normally the pressure was set at 10um but films were deposited at pressures as high as 100um.

The hysteresis loops for the normal component of the magnetization were made by observing the Hall effect in these films [9]. All measurements were taken at room temperature. A square Hall probe configuration was used; this configuration probed a film area of 64 sq. mm. The maximum Hall current, I_{hall}, used was 100ma, however, lower currents were used for the films thinner than .5um to avoid heating effects. The Hall current was supplied by a current regulated power supply and the Hall voltage, V_h, generated was displayed on a x-y plotter. The saturation values of the Hall voltage were taken as $\pm M_\perp/M_s = \pm 1$. The magnetic field was produced by a 4 inch adjustable gap electromagnet and the field was measured by a

semiconductor Hall probe.

The film magnetization was determined by using the stripe period, P_o, the film thickness, h, and the information obtained from the normal Hall hysteresis loop. The normal Hall hysteresis loop gives 1) the normalized initial susceptibility, $(4\pi\chi_i/4\pi M_s)=(1/4\pi M_s)\cdot d(4\pi M_\perp)/dH|_{H_\perp=0}$, 2) the normal field, $H_\perp(.5=M_\perp/M_s)$, needed to produce $4\pi M_\perp=.5(4\pi M_s)$, and 3) the bubble collapse field, H_{col}. The collapse field and $H_\perp(.5=M_\perp/M_s)$ are used to determine $4\pi M_s$ by the method of Shaw, et. al. [32]. The normalized initial susceptibility is used to find the magnetization from the relationship between $4\pi\chi_i$ and the characteristic length, ℓ [33]

$$4\pi\chi_i = 1 + 7.12\ell/h$$

by

$$4\pi M_s = (4\pi\chi_i/4\pi M_s)/(1 + 7.12\ell/h).$$

The magnetization values found by these methods agree to within 10%. In all subsequent calculations, the average of these magnetizations is used.

Accurate thickness measurements (<300Å error) were made by using an interferometer while x-ray fluorescence was used in determining the composition. A typical deposition lasted 4 hours and resulted in films about .75um thick.

Stripe periods for the films with low coercivity and observable stripes were either measured directly by using polar Kerr contrast microscopy and visually measuring the stripe periods or photographing the films and determining the stripe periods from the prints. The characteristic lengths were determined from the zero field stripe period and the film thickness [32].

Previously, the anisotropy fields of GdCo, GdCoMo and GdFe amorphous bubble films have been determined from in-plane M-H loop traces made on high drive inductive loop tracers [19] and from hysteresis loops made on

a vibrating sample magnetometer [22]. The in-plane nucleation field was taken as $H_k-4\pi M_s$ by Kobaliska, et. al. [19] and the in-plane saturation field as H_k by Kobayashi, et. al. [22] respectively. Assuming that the nucleation or the saturation field is $H_k-4\pi M_s$ or H_k respectively does not account for the energy dissipated in moving the domain walls such as those seen in hard axis hysteresis loops of garnet materials [34]. Opening of in-plane loops for amorphous GdCo bubble films have been reported by Lee and Soohoo indicating that domain walls are also moved during in-plane hysteresis traces for these films [35].

To eliminate the error inherent in assuming that the saturation field or the nucleation field is H_k or $H_k-4\pi M_s$ respectively, a technique is described to give the correct value of $H_k-4\pi M_s$ for uniaxial anisotropic amorphous magnetic bubble films.

The anisotropy can be determined from longitudinal susceptibility measurements with a transverse field. Shumate, et. al. [36] suggested and demonstrated this technique with garnet bubble materials. In this susceptibility measurement technique the magnetization is pulled in-plane to its hard axis by a strong d.c. field, H_{dc}, then a small a.c. drive field, h_{ac}, is added in the normal direction, the easy axis direction. The a.c. component of the magnetization normal to the film, m_{ac}, is then measured. The susceptibility, χ, measured will be [36]

$$4\pi\chi=4\pi m_{ac}/h_{ac}=4\pi M_s/[H_{dc}-(H_k-4\pi M_s)] \quad \text{for } H_{dc}>H_k-4\pi M_s \quad \text{eq. 1a.}$$

$$4\pi\chi=4\pi m_{ac}/h_{ac}=4\pi M_s\cdot H_{dc}^2/\{[(H_k-4\pi M_s)^2-H_{dc}^2][H_k-4\pi M_s]\}$$

$$\text{for } H_{dc}<H_k-4\pi M_s \quad \text{eq. 1b.}$$

if the sample is in the single domain state and it has no damping or non-uniformities. The susceptibility should show a peak near $H_{dc}=H_k-4\pi M_s$. Bubble materials will probably be in the multidomain state if $H_{dc}<H_k-4\pi M_s$; however, for $H_{dc}>H_k$ the sample is in the single domain state and equation 1a holds. Starting from $H_{dc}>>H_k-4\pi M_s$ and decreasing H_{dc}, the susceptibility should increase. For the garnet materials it increases and reaches a maximum near $H_{dc}=H_k-4\pi M_s$ where the sample breaks into the multidomain state and the susceptibility levels off [36,8]. Shaw, et. al. have taken the point where it breaks into the multidomain state as $H_k-4\pi M_s$ [8]; this may not be correct or even a good assumption for all bubble materials. The correct method is to extrapolate from the high field susceptibilities the d.c. field which would give an infinite susceptibility. The extrapolated infinite susceptibility field can be easily found by plotting the inverse of the susceptibility versus the in-plane field. From equation 1a the inverse of the high field susceptibility, $1/4\pi\chi$, is

$$1/4\pi\chi=h_{ac}/4\pi m_{ac}=[H_{dc}-(H_k-4\pi M_s)]/4\pi M_s$$

The inverse of the high field susceptibility should be a straight line which extrapolates to zero at $H_{dc}=H_k-4\pi M_s$. Since the zero field intercept is found the scaling of χ and $1/\chi$ is arbitrary as long as it is linear.

Shumate measured the longitudinal susceptibility for garnet bubble materials by using the Faraday effect to detect the normal component of the magnetization. However, for the longitudinal susceptibility measurements in GdFe films the Hall effect and the polar Kerr effect offer the means of measuring the a.c. magnetization component normal to the film. The Hall effect has several advantages over the polar Kerr effect. First, large signal to noise is easily obtained from the Hall effect, second, tests

can be performed in a lighted room, and third, a conventional electromagnet may be used without modifying the pole pieces. The Hall effect technique has the disadvantage that electrical contact must be made to the films. Thus the Hall effect is better suited for materials research while the polar Kerr effect may be better for production purposes.

The Hall effect susceptibility system used is shown in figure 11. A typical susceptibility trace is shown in figure 12a and the inverse is shown in figure 12b. From figure 12b, $H_k-4\pi M_s$=200e. For this technique, the error is estimated to be about $\pm$70e for $H_k-4\pi M_s$ provided $H_k-4\pi M_s>0$; this error is comparable to that found by Shumate, et. al. for garnets [36]. Shumate, at. al. report a room temperature anisotropy field and magnetization of 4800$\pm$75oe and 225G respectively for $Er_2Eu_1Ga_{0.7}Fe_{4.3}O_{12}$.

Figure 12a also shows that the film breaks into the multidomain state at a much higher field than $H_k-4\pi M_s$. Muller [37] calculated that the domain nucleation field, H_n, for an ideal uniaxial thin film should be close to H_k. This is seen here because $H_n\simeq$1250e and H_k=1370e even though $H_k-4\pi M_s$=200e.

During the sputter deposition of thin films argon gas atoms get trapped in the films. Argon atomic fractions as high as 8 atm % are reported by Wagner, et. al. [38] for bias sputtered GdCo films. The argon fractions are determined for the films made here to find the effect of the argon on the saturation magnetization, the iron moment value and the exchange properties and calculations.

The argon content in the GdFe films is found by assuming that only three elements (iron, gadolinium, and argon) are in the films and that no voids or vacancies exist in the films. Let P_i be the volume fraction of the i^{th} element in the film. By the above assumption, we get:

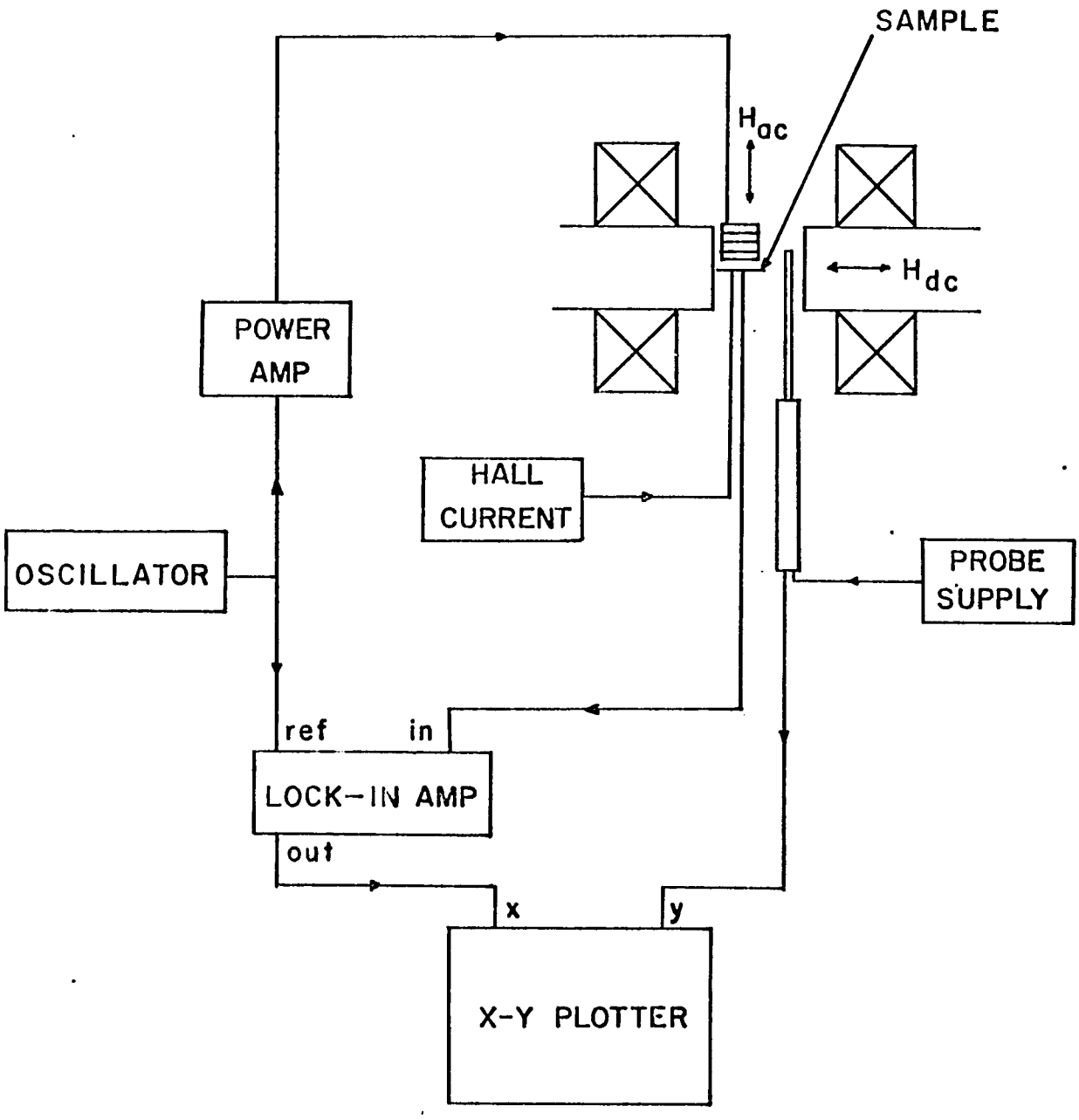

Figure 11: Susceptibility measurement system: this system is used to measure the anisotropy fields for GdFe amorphous films.

Figure 12a.

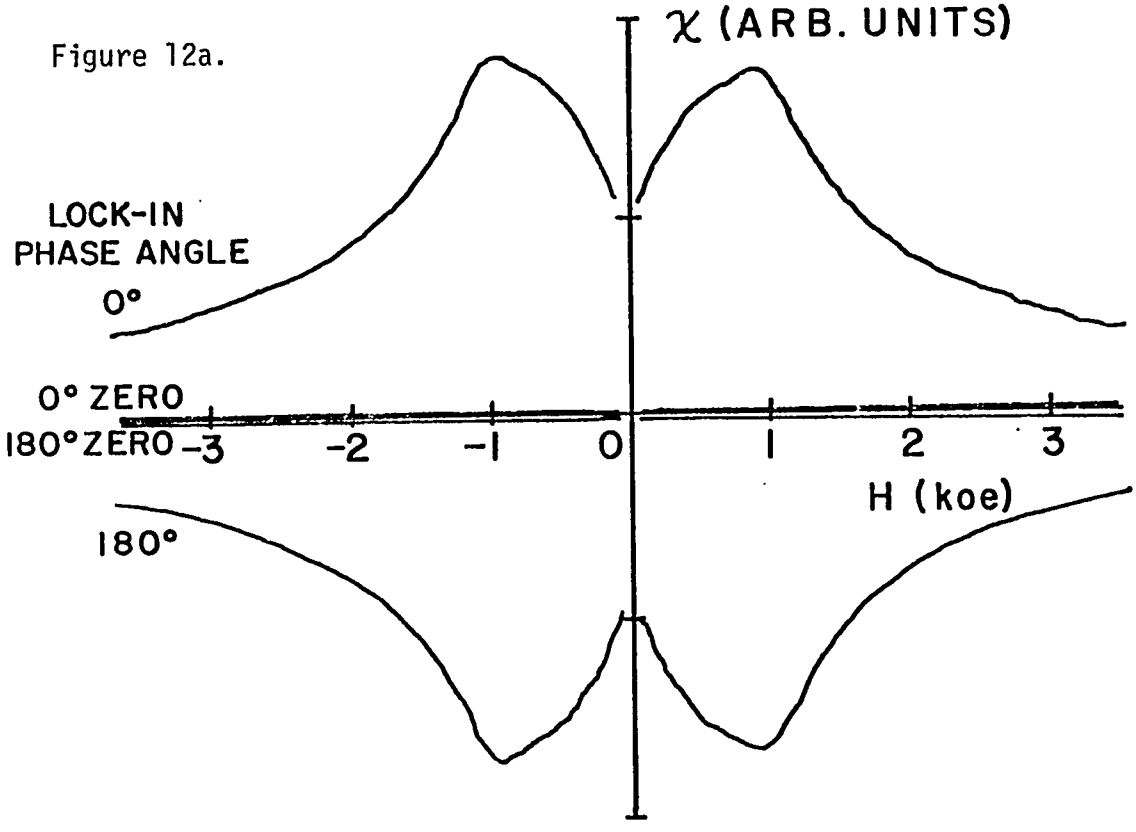

Figure 12b.

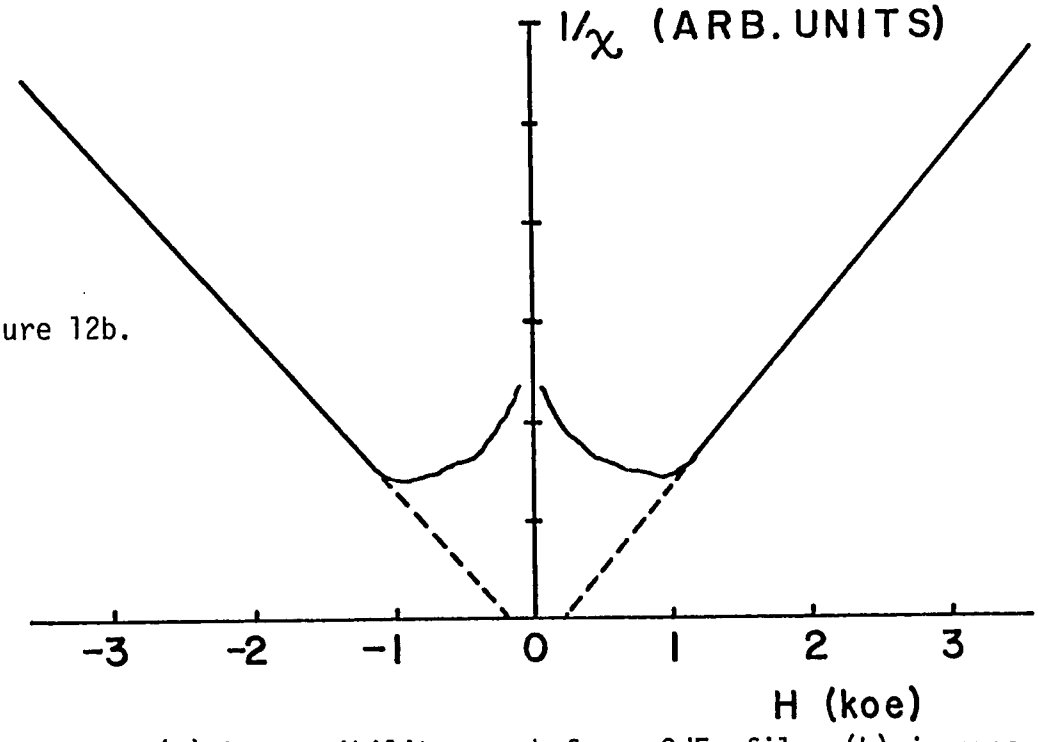

Figures 12a&b: (a) Susceptibility graph for a GdFe film, (b) inverse of 12a.

$$\Sigma P_i = 1 = P_{fe} + P_{gd} + P_A$$

then $$P_A = 1 - P_{fe} + P_{gd}$$

Also, a thin film x-ray fluorescence approximation is assumed; in this approximation the number of counts on the characteristic line of the i^{th} element is proportional to the amount of the i^{th} element in the film. The proportionality constant is determined by measuring the counts on a pure standard of the i^{th} element. Let N_{fi} be the counts on the film on the line of the i^{th} element, t_f be the actual thickness of the film, t_{stdi} be the thickness of the standard of the i^{th} element, N_{stdi} be the counts on the i^{th} standard and t_{effi} be the effective thickness of the i^{th} element in the sample. The x-ray fluorescence thin film approximation says, for samples with the same surface area measured, that the number of counts per unit thickness is a constant. The thin film approximation gives:

$$N_{stdi}/t_{stdi} = N_{fi}/t_{effi} = N_{fi}/P_i t_f$$

by using the volume fraction definition. Then

$$P_i = N_{fi} t_{stdi}/t_f N_{stdi}$$

The number of counts referred to above is the actual counts, I, less the background counts, I_{bk}.

$$P_i = (I_{fi} - I_{bki}) t_{stdi}/[t_f (I_{stdi} - I_{bki})]$$

In the film, the number of atoms of the i^{th} element per unit volume is

$$n_i = P_i A_v p_i / AtmW_i$$

where A_v is Avagadro's number, p_i is the density of the i^{th} element in bulk, and $AtmW_i$ is the atomic weight of the i^{th} element. The atomic fraction of the i^{th} element in the film is

$$Atm\%_i = n_i/\Sigma n_i = \frac{P_i p_i/AtmW_i}{\Sigma P_i p_i/AtmW_i} \qquad \text{eq. 2}$$

For this composition determination technique to be used the actual thickness of the film must be known, the actual counts on all of the elements in the film and in the standards. This technique assumes that the difference between the actual thickness of the film and the sum of the effective thicknesses of the counted elements is due to the unmeasured element present.

For GdFe films with argon assumed as the only remaining element present, equation 2 becomes

$$Atm\%A = \frac{P_A \cdot 2.135}{P_{fe} \cdot 8.497 + P_{gd} \cdot 3.044 + P_A \cdot 2.135}$$

and the maximum possible error is

$$\frac{\Delta Atm\%A}{Atm\%A} = d \cdot Atm\%Fe \cdot [0.749 + 0.251/Atm\%A] + d \cdot Atm\%Gd \cdot [0.299 + 0.701/Atm\%A]$$

where $d \simeq .15$ and is due to an additive 5% uncertainty in the actual counts on the Fe and on the Gd lines and to a 5% uncertainty in the thickness.

The differences in the composition analysis just described and the analysis method used to determine x of Fe_xGd_{1-x} are 1) the Fe_xGd_{1-x} method gives the x-ray thickness due to the elements counted only, in this case, $t \simeq \Sigma t_{effi}$, while the just described method uses the actual thickness in its

composition calculations and 2) the Fe_xGd_{1-x} method gives the composition in terms of just the elements measured while the just described method requires that the remainder of the film is assumed to be composed of another element. It should be noted at this point that the Fe_xGd_{1-x} method uses a linear approximation for the density of the film. A linear density dependence on the atomic fraction of the measured elements is observed for GdCo films [39] and is thus used in the effective thickness analysis described in the Fe_xGd_{1-x} method. The linear density has little effect on the Fe_xGd_{1-x} calculations since ρ_{gd}=7.95 gm/cc and ρ_{fe}=7.88 gm/cc, less than 1% difference.

CHAPTER IV: RESULTS AND DISCUSSION

In order to study the effects of substrate bias and argon pressure on the wall energy and anisotropy properties of GdFe films, films were made under three different bias and pressure conditions. For several target compositions and argon pressures the substrate bias ranges were found which gave suitable compositions and magnetic properties for stripe domain films.

A) Stripe Periods:

The stripe periods measured for GdFe films are shown in figure 13 along with a curve representing the stripe periods given by Kobaysahi, et. al. [22]. Stripe period measurements can be made in the magnetization region which produces observable and low coercivity stripes, $400G \tilde{<} 4\pi M_s \tilde{<} 1100G$. The stripe periods of our films are smaller than the stripe periods given by Kobayashi, et. al. for films of the same magnetization and show a more rapid decrease with increasing magnetization than those of Kobayashi, et. al. Bias and pressure appear to have an effect upon the stripe periods but not to the extent of producing the large stripes observed by Kobayashi, et. al., see figure 13. Larger stripe periods are, however, observed for films made at -100vdc bias than at -70vdc bias for films of similar magnetization.

B) Characteristic Length and Wall Energies:

The characteristic length can be found by using the stripe period, the film thickness and the conversion tables by Shaw, et. al. [32]. The characteristic lengths versus $4\pi M_s$ are shown in figure 14 for films deposited at -70vdc and -100vdc substrate biases. A fitted curve to the characteristic length data of the GdFe films made at -70vdc bias gives the equation $\ell = 2.90/(4\pi M_s)^{1.96}$ where ℓ is the characteristic length in centi-

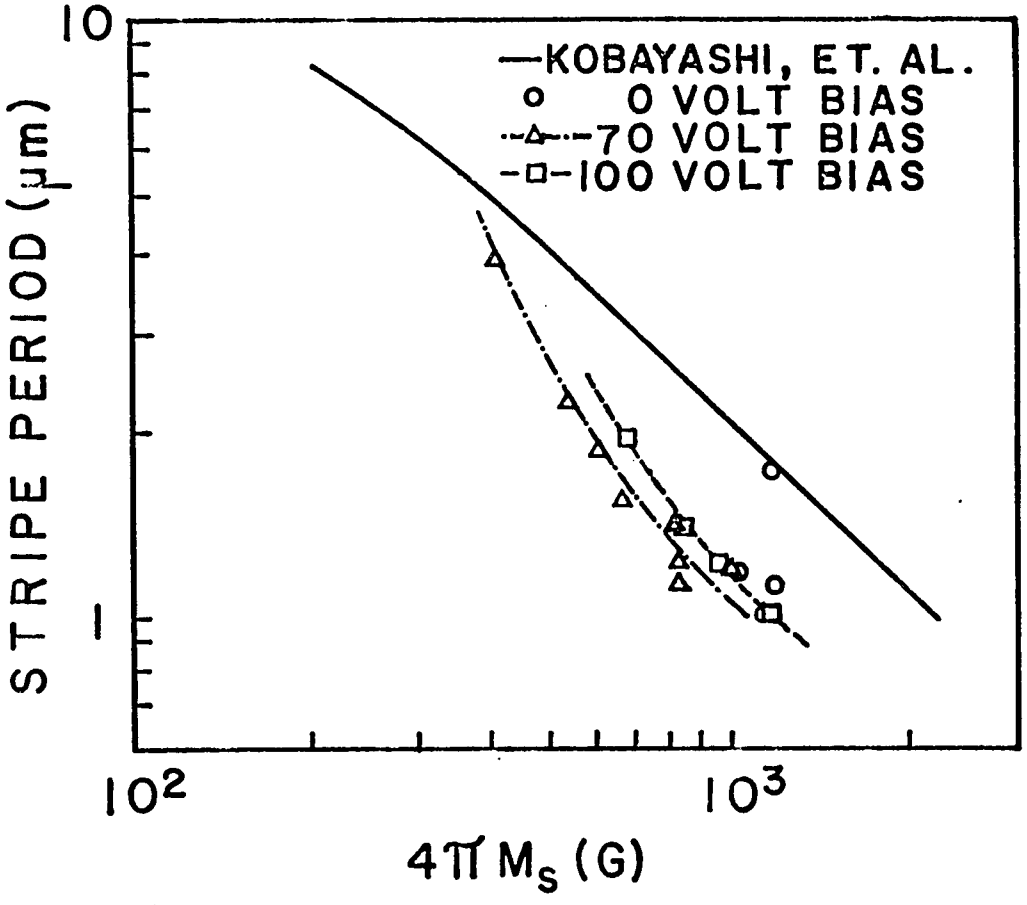

Figure 13: Stripe period data for bias sputtered GdFe films. The stripe periods are smaller than reported for the similar magnetization films of Kobayashi, et. al. [22].

meters and $4\pi M_s$ is the magnetization in Gauss. The exponent of $4\pi M_s$, 1.96, indicates that films made at -70vdc bias closely follow a constant wall energy curve since the characteristic length is defined [40] as

$$\ell = 4\pi\sigma/(4\pi M_s)^2.$$

Very little difference between the fitted curve, $\ell = 2.90/(4\pi M_s)^{1.96}$, and $\ell = 4\pi(.29)/(4\pi M_s)^2$, a constant wall energy curve for $\sigma = .29 erg/cm^2$, can be seen in the range of observable and low coercivity stripes. Films made at -100vdc substrate bias tend to have higher wall energies than films made at -70vdc. A curve fitted to the characteristic length data of films made at -100vdc gives $\ell = 1.63/(4\pi M_s)^{1.82}$. The fitted curve is close to the constant wall energy curve of $\sigma = .46 erg/cm^2$. Both of these curves are shown in figure 14.

The wall energies are plotted in figure 15. The average of the wall energies for the films made at -70vdc and -100vdc are within the respective experimental errors for all but one of the films examined.

Due to sputtering system contamination problems associated with grounded bias sputtering, only one set of films were made at 0vdc bias. These films are closely spaced in magnetization and in wall energies thus no trend can be discerned for films made at 0vdc. The range of wall energies of the films made at 0vdc is from .37 to .45 erg/cm^2, which is between the wall energies of films made at -70vdc and -100vdc bias.

Using a film thickness of 1.25um [22] the stripe period versus magnetization data of Kobayashi, et. al. can be converted to characteristic length versus magnetization data. The characteristic lengths found are also presented in figure 14. The characteristic lengths, found from the data, are greater than the characteristic lengths found here for bias sputtered

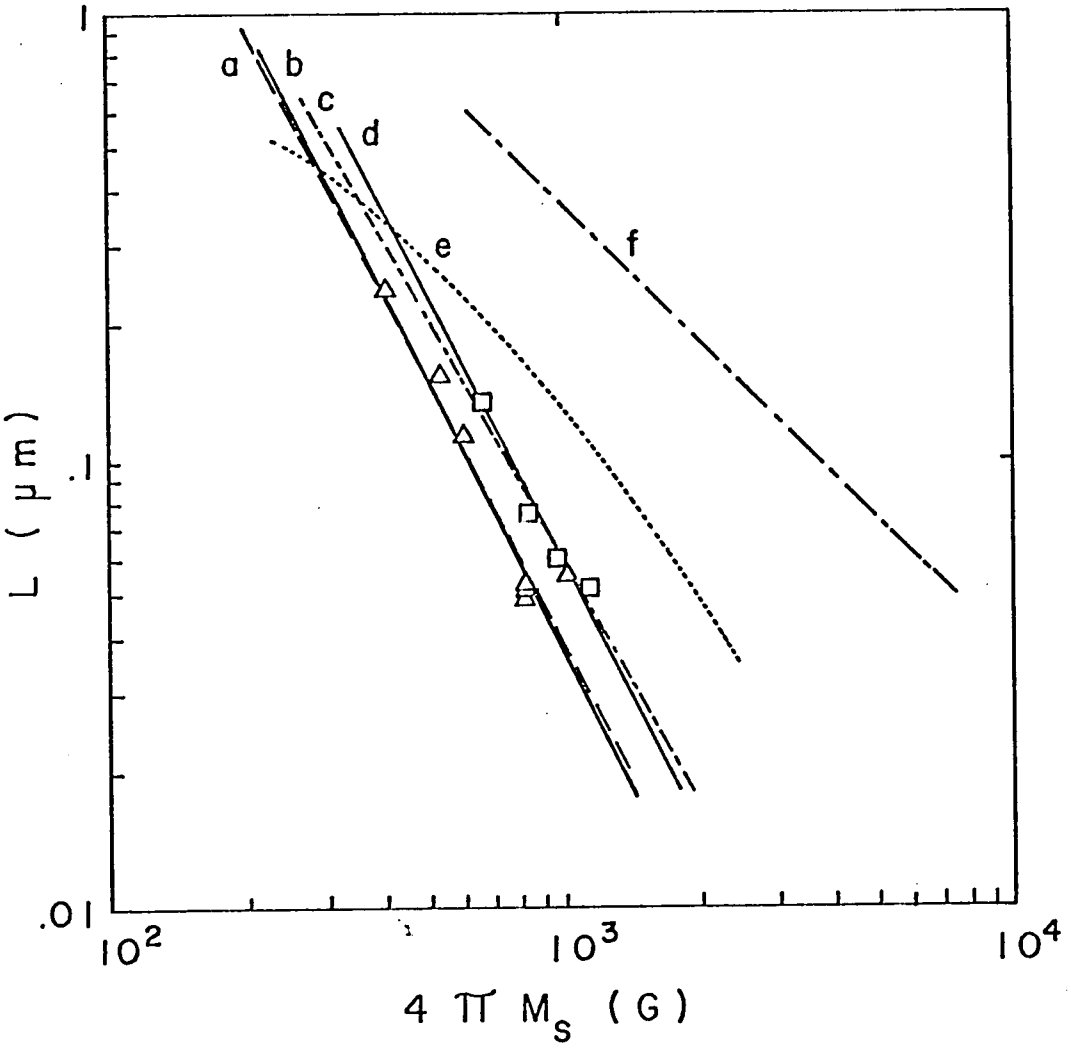

Figure 14: Characteristic length versus magnetization: (a) -70vdc substrate bias, (b) σ_w=.29erg/cm^2, (c) -100vdc substrate bias, (d) σ_w= .46erg/cm^2, (e) for GdFe films of Kobayashi, et. al. [22], (f) for GdCo films of Chaudhari, et. al. [17].

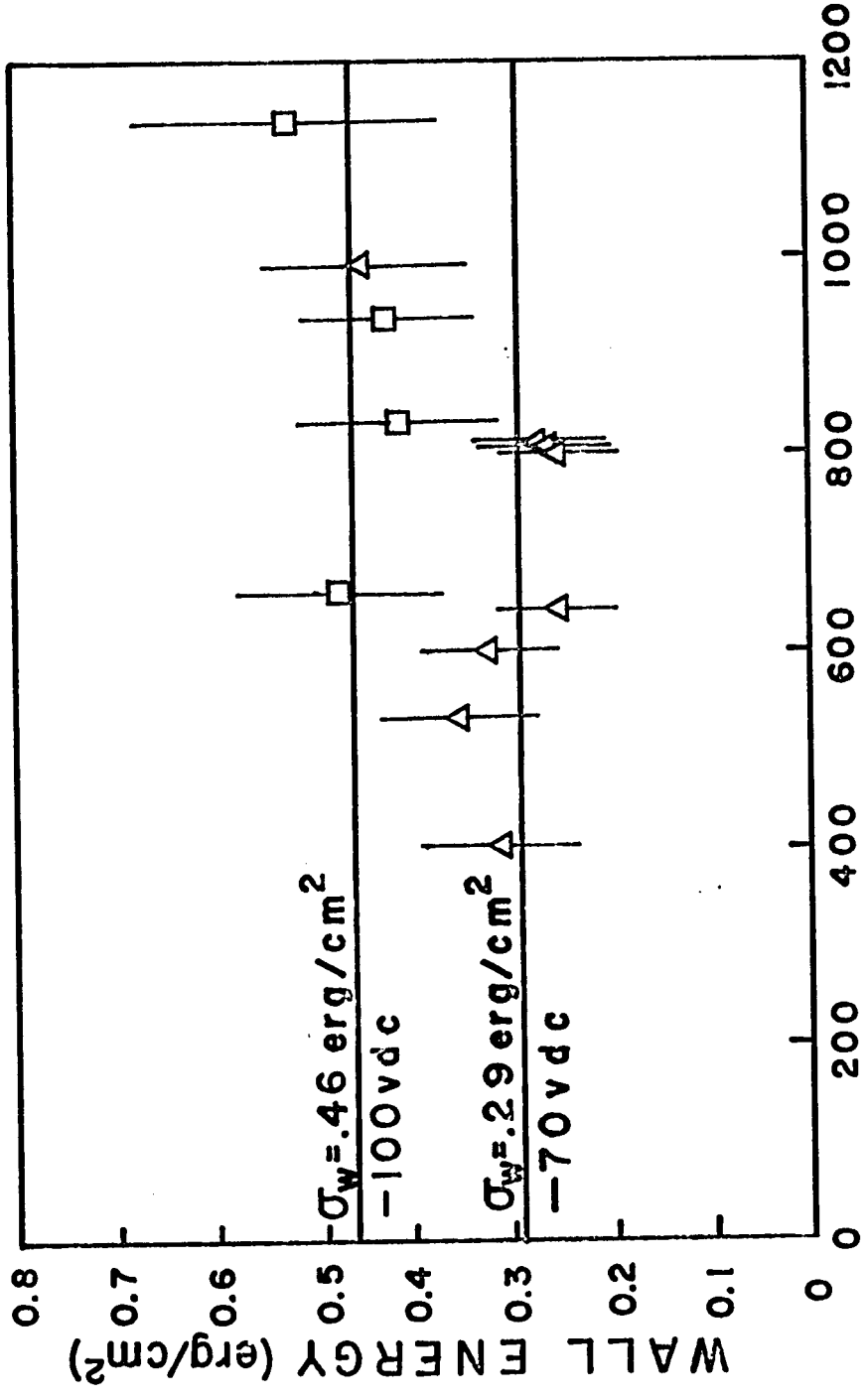

Figure 15: Domain wall energy dependence on magnetization for bias sputtered GdFe films.

films of similar magnetization.

The dependence of the characteristic length on magnetization can be described by $\log \ell = \log \ell_0 + s \cdot \log 4\pi M_s$ where s is the slope of the $\log \ell$ versus $\log 4\pi M_s$ curve. A slope of s=-2 would indicate a wall energy independent of magnetization, however, a dependence with s>-2 indicates that the wall energy increases with magnetization. A s=-1 slope would indicate a linear dependence of wall energy on the magnetization.

A discussion of the wall energy dependencies of sputtered GdFe and sputtered GdCo films is presented here. From figure 14, s≃-2 for our films, s≃-1 for the GdCo films of Hasegawa, et. al. [6], but s varies from -.75 to -1.3 for the sputtered GdFe films of Kobayashi, et. al. A s≃-1 dependence is also observed for GdCoX sputtered films in the composition ranges where stripe domains are observed for the films of Chaudhari, et. al. [17]. The composition, magnetization, and wall energy of GdCo and GdCoX films are controlled by the substrate bias during the deposition. The use of substrate bias to control composition leads to a wall energy dependence on composition and hence on magnetization. This could explain the s≃-1 characteristics of GdCo and GdCoX films. No explanation is given for the dependence of wall energy on $4\pi M_s$ observed for the data of Kobayashi, et. al.

C) Anisotropy Fields and Energies:

The anisotropy field data, H_k, versus $4\pi M_s$ are shown in figure 16 for our films and for the films of Imamura, et. al. [23]. $H_k' = H_k - 4\pi M_s$ was determined by the susceptibility technique described in the experimental procedure chapter and the magnetization was determined by bubble statics. In the range studied there does not appear to be any trend in H_k with $4\pi M_s$ for our films made at 0vdc, -70vdc or -100vdc substrate bias. Also, no anisotropy energy, K_u, dependence on magnetization can be seen. The uniaxial

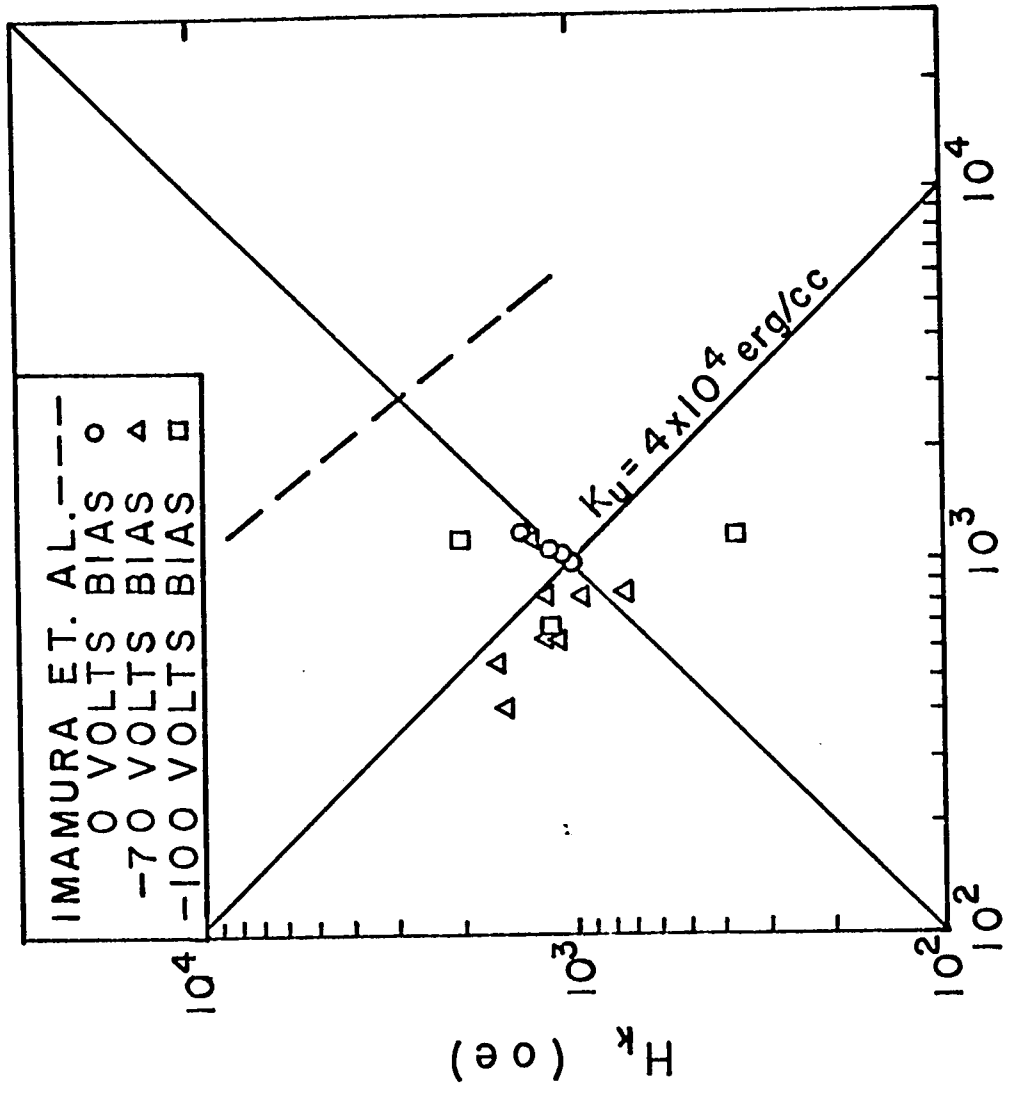

Figure 16: Anisotropy field dependence on magnetization. The data presented is about an order of magnitude lower in energy than reported by Imamura, et. al. [23].

anisotropy energies vary from 4.0 to 5.0×10^4erg/cc with an average of 4.4×10^4erg/cc for films made with 0vdc, from 2.4 to 5.6×10^4erg/cc with an average of 3.4×10^4erg/cc for films made at -70vdc and from 1.7 to 8.8×10^4 erg/cc with an average of 4.5×10^4erg/cc for films made at -100vdc.

The average K_u of the films made at -100vdc is 32% higher than the average K_u of films made at -70vdc. However, there is a wide range of K_u values for films made at -100vdc, this makes the interpretation of the anisotropy dependence on bias difficult. An anisotropy dependence on bias is expected since 1) the exchange constant should vary little throughout the composition range where stripes can be observed and 2) the average wall energy of films made at -100vdc are higher than the average of the films made at -70vdc. However, the anisotropy dependence on bias needed to fully explain the wall energy dependence on bias is not seen.

The wall energies of films made at a given bias are nearly the same, but the anisotropy energies vary considerably. This would suggest that the exchange constant varies as the inverse of the anisotropy. However, such an interpretation is not considered to be physically acceptable because the films are nearly the same composition and the exchange constant values should be close. Also a linear dependence of the wall energy squared on the anisotropy energy is seen; this implies that the exchange stiffness is essentially a constant in this range. Further discussion on the exchange constant is given later in this chapter.

The reported anisotropy energies of films made by Imamura, et. al. are as high as 3×10^5erg/cc which is about ten times the anisotropies reported here. Also reported by Imamura, et. al. is a linear increase in K_u with magnetization for films with $4\pi M_s \tilde{<} 1000$G and then a gradual decrease in K_u for the films with $4\pi M_s \tilde{>} 1000$G.

GdFe films made at 0vdc substrate bias are reported in figure 16 to

show that 1) stripe domains can exist in films made at 0vdc bias and 2) that they have wall energies and anisotropies close to the wall energies and anisotropies of films made at -70vdc and -100vdc bias.

D) Anisotropy Mechanism:

In evaluating a thin film material for bubble material purposes it is important to know the cause of the anisotropy which orients the easy axis normal to the plane of the film.

X-ray diffraction studies of sputtered GdFe films show these GdFe films to be amorphous, see figure 17. This test rules out magnetocrystalline anisotropy as the anisotropy mechanism in these films.

Another form of anisotropy found in thin films is structural or shape anisotropy due to columnar or longitudinal growths [24,41]. However, it should be pointed out that shape anisotropy alone cannot produce enough anisotropy for $K_u > 2\pi M_s^2$. $K_u > 2\pi M_s^2$ is a requirement for magnetic thin films to support the magnetization normal to the film.

Considerations should be given 1) to substrate bias effects during sputtering and 2) to the properties of evaporated GdFe and GdCo films when studying the anisotropy mechanism of bias sputtered GdFe films.

GdCo films are found to have insufficient normal anisotropy to support support stripe domains if deposited by sputtering with 0vdc substrate bias [7,16] or by evaporation [42,43]. Since GdFe films deposited by sputtering at 0vdc bias and GdFe films deposited by evaporation [3,29] can have $K_u > 2\pi M_s^2$, then an anisotropy mechanism must be present in GdFe films that is not present in GdCo films. Sputtered GdCo films and sputtered GdCoMo films are postulated to have cobalt ordering induced by bias sputtering as the anisotropy mechanism. Evaporated GdCo films are shown to be non-magnetostrictive [42] when strained in a M-H loop tracer; then substrate

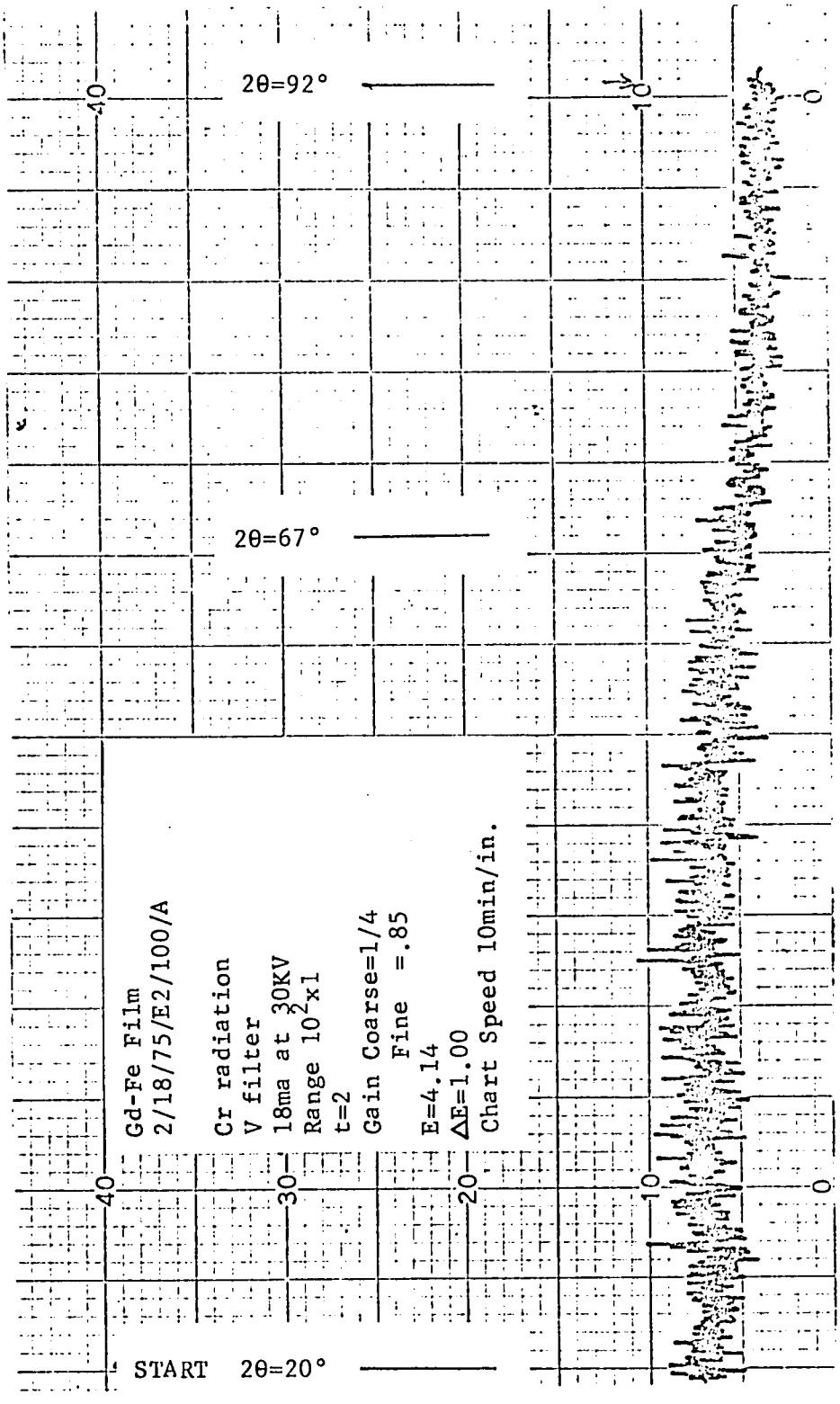

Figure 17: Diffractometer curve for an amorphous GdFe film. No evidence of crystallinity is seen.

induced external stress does not affect the anisotropy. The anisotropy mechanism whereby the anisotropy is caused by stress is called the inverse magnetostrictive effect. Thus, using bias sputtering arguments and the properties of evaporated GdCo films, inverse magnetostriction may be the anisotropy mechanism present in GdFe films that is not present in GdCo films. However, it should be noted, at this time, that moment ordering or shape effects are not excluded as anisotropy mechanisms in the GdFe films made here.

To further investigate the cause of the anisotropy in the GdFe films made here, films which have stripe domains are examined using polar-Kerr contrast microscopy. A sputtered GdCo film is also examined for comparison. GdFe samples and a GdCo sample which have film parts detached from the glass substrates are examined. Figure 18a is a photomicrograph of a GdFe film. The film has slightly coercive stripe domains in the film region that is adhering to the substrate while no stripes are observed in the part of the film that has broken loose from the substrate. No domain structure could be observed on any detached GdFe film part. The part of the film that has broken loose from the substrate in figure 18a forms a bulge indicating that compressive stress is relieved in the detached part of the film. Since no stripe domains can be seen in the part of the film where substrate induced stress has been relieved, inverse magnetostriction is believed to be the dominant anisotropy mechanism in these GdFe films. This is in sharp contrast to that observed for GdCo films [4], also see figure 18b. The GdCo film in figure 18b, made under similar deposition conditions, is also found to be under compression because the detached part of the film bulges up from the substrate similar to the detached part of the GdFe film of figure 18a. The stripe domains in the

Figure 18a: a GdFe film

Figure 18b: a GdCo film

Figure 18a&b: Substrate stress effects on (a) GdFe film and (b) GdCo film. Detached part of each film is the right part of each photograph.

GdCo film, however, still exist in the part of the film that is detached from the substrate. It should also be noted that the stripe period in the detached part of the film is the same as the stripe period in the adhered part of the film, to within measurement accuracy. This indicates that inverse magnetostriction does not make a significant contribution to the anisotropy of GdCo films made under similar deposition conditions to the GdFe films made here.

An estimate of the anisotropy energy fraction due to inverse magnetostriction can be obtained by realizing that the minimum observable stripe period is about 1um while the stripe period of the part of the GdFe film in figure 18a that remains attached to the substrate is P_o=5.4um. The film thickness, h, is .75um; then P_o/h=7.2, ℓ_1/h=.433 and ℓ_1=.325um. At the minimum observable stripe period, P_o=1.0um, P_o/h=1.33, ℓ_2/h=.0572 and ℓ_2=.0429um. The conversion of P_o/h to ℓ/h was found by using the tables of Shaw, et. al. [32]. Using these two values of characteristic length, the minimum fractional change in the anisotropy can be found by

$$\Delta K/K = 1 - \ell_2^2/\ell_1^2$$

from $\sigma=4\sqrt{AK_u}$ and $\ell=\sigma/(4\pi M_s^2)$. The subscripts 1 and 2 are associated with the attached and the detached parts of the film respectively. For the film in figure 18a the minimum fractional change in the anisotropy is:

$$\Delta K/K|_{min} = 1 - (.0429um)^2/(.325um)^2 = .983$$

For the GdCo film in figure 18b, the observed stripe period is 4.5$\pm$.2um for both the attached and the detached parts of the film. The maximum fractional contribution to the anisotropy is due to the stripe period measurement accuracy of .2um. for this GdCo film, h=1.9um,

$P_o/h=2.37$, $\ell_1/h=.1439$, $\ell_1=.273um$ for $P_o=4.5um$ and $P_o/h=2.26$, $\ell_2/h=.1346$, $\ell_2=.256um$ for $P_o=4.3um$. This gives a maximum fraction change in the anisotropy due to inverse magnetostriction for this GdCo film of

$$\Delta K/K|_{max} = 1 - (.256um)^2/(.273um)^2 = .12$$

Thus over 98% of the anisotropy is stress induced in this GdFe film while less than 12% of the anisotropy is due to stress in this GdCo film.

At this point, the discussion will digress from inverse magnetostriction and focus upon the stress and strain in the deposited films. As can be seen in figures 18a&b and from the above discussion of the figures, the films are in compression; however, added proof is presented 1) to confirm that these films are in compression and 2) to estimate the levels of stress and strain in a film. Using the stress levels found and the anisotropies observed, the magnetostriction coefficient can be estimated.

The stress levels in the films are found by using the method described by Glang, et. al. [44] for molybdenum films bias sputtered onto silicon wafers. The surface of a GdFe film is determined by using an interferometer; then the film is removed and the profile of only the substrate is taken along the same path. The bowing of the substrate due to the presence of the film can be found by the analysis of Glang, et. al. Figures 19a&b show the observed surface profiles along two orthogonal in-plane directions for both the film and the substrate. Using the difference in the two profiles and accounting for the difference due to the interferometer tilt, displacement profiles along the two measurement directions are determined. The displacement profiles are shown in figure 20. Note that the film bows the substrate such that the surface of the substrate with the film on it is more convex than the same surface without the film. This indicates

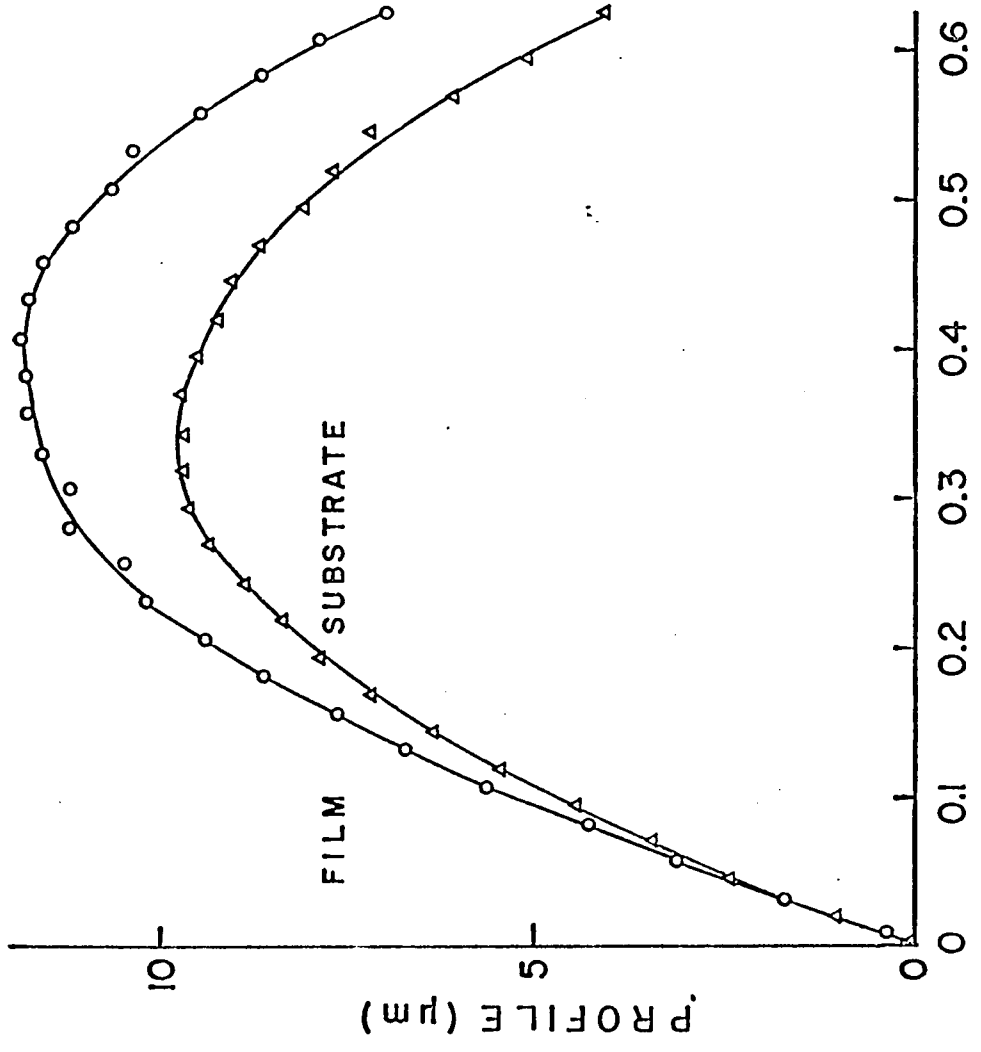

Figure 19a: Surface profile of a glass substrate and the same substrate with a sputtered GdFe film.

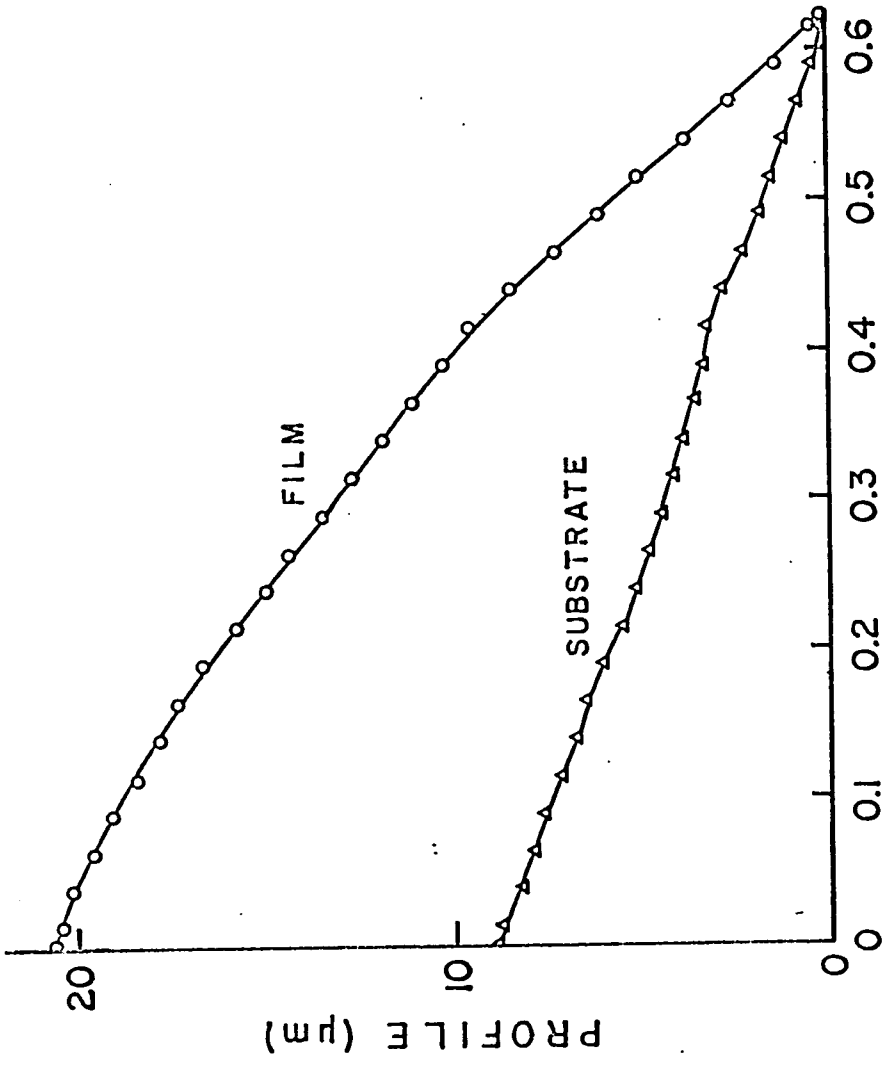

Figure 19b: Same film described in Figure 19a except the surface profiles are measured along an orthogonal in-plane direction to Figure 19a.

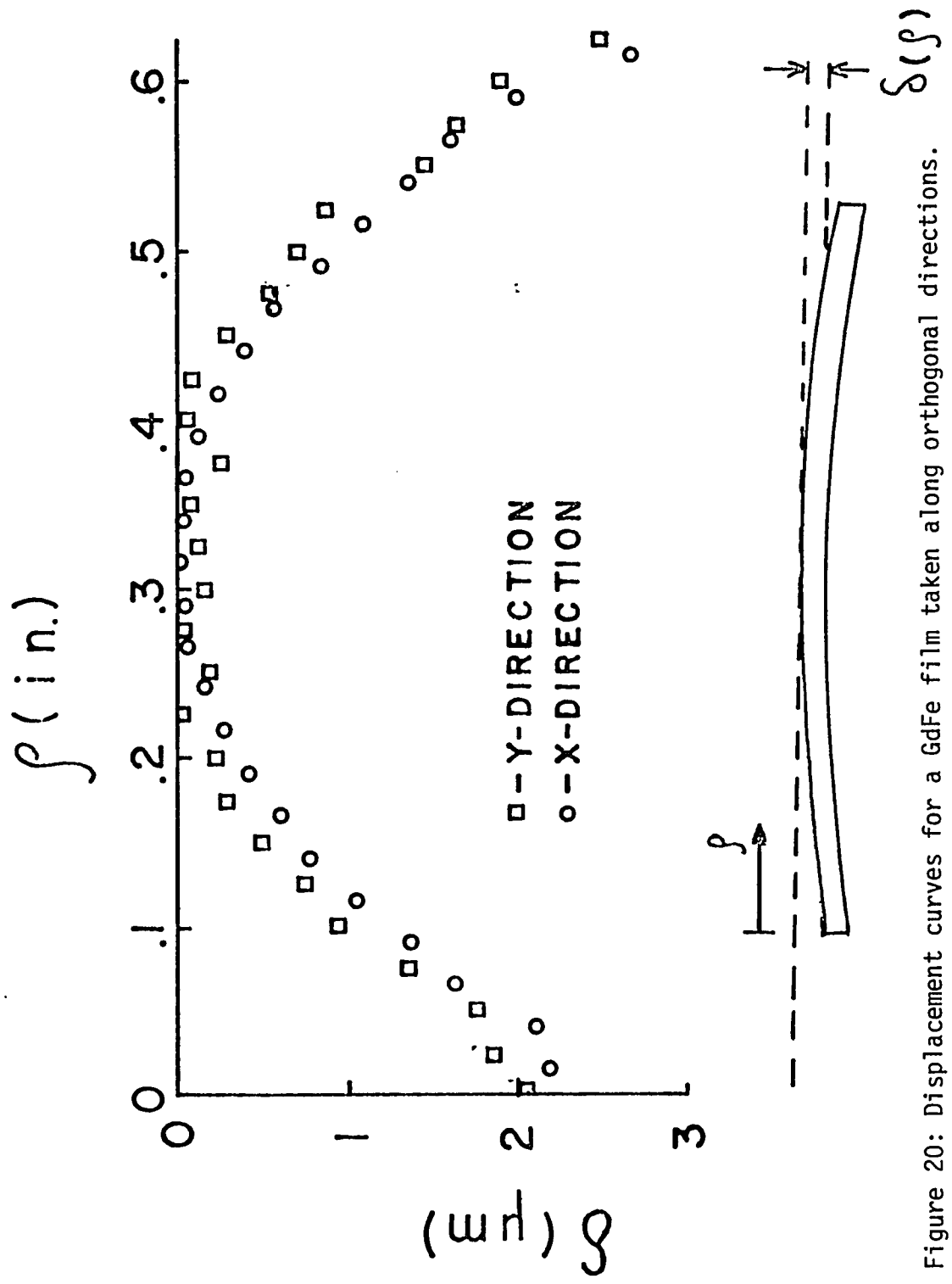

Figure 20: Displacement curves for a GdFe film taken along orthogonal directions. The displacement curves indicate an isotropic in-plane compressive stress.

that when the film is on the substrate, the film is in compression and, of course, the substrate is in tension. The parabolic-like nature of the displacement profiles tend to indicate that the film is under isotropic in-plane compression. Using the equation for the stress of a film rigidly held by the edges, equation 2 of Glang, et. al., the stress in the film is estimated to be $7.6 \times 10^9 \text{dyne/cm}^2 = 110 \text{kpsi}$. This is a tremendous stress level; probably high enough to cause plastic deformation in the film. However, such stress levels are reported for evaporated thin films [44] and for sputtered films [44,46].

The strain in the films is found by observing parts of the film that become detached from the substrate and estimating the strain. Only circular isolated areas that are detached from the substrate are examined. This type of detached film forms a domed sphere-like structure. Approximating the structure as a section of a sphere, the average strain in the attached film is crudely approximated by $\langle e \rangle = -(\delta/r)^2/2$ where δ and r are the height and radius of the bubble respectively. The part of the film that is detached from the substrate is considered to be unstressed and to possess little remanent strain. See appendix for the development of the average strain approximation.

Detached film bubbles were examined in various parts of a film made at the same time as the film on which the stress analysis was made. The bubbles ranged in size from 24 to 48um in diameter and from 1.6 to 3.3um high. The range of the $(\delta/r)^2$ values was from .0126 to .0184 with an average of .016. This gives an average strain of $\langle e \rangle \simeq -.008$ when the film is attached to the substrate. A strain of -.008 is probably beyond the elastic limit if these films. Thus the crudeness of the approximation used in evaluating the average strain is considered to be justified.

A strain of -.008 for a compressive stress of 110kpsi is comparable to an unannealed stainless steel strained beyond the elastic limit; but, an estimated Young's Modulus is $1x10^{12}$dyne/cm^2 which is reasonable for metals.

The usual explanation for the cause of stress in thin films is the strain induced by the difference in thermal contraction effects of the substrate and the film after the deposition of the film. Preliminary data by C. T. Chen, of this laboratory, indicates that the deposition temperature during the bias sputter deposition is about 100°C for the sputtering system used to make the GdFe thin films for this investigation. For Corning 0211 microsheet ® substrates [31] with iron films this would correspond to a thermal contraction difference of only $+3.2x10^{-4}$in./in. with the film in tension. This is quite different from the -.008 observed. This indicates that there must be another cause of strain in these films. Although the origin of this strain is still unknown, the points that 1) the films are under considerable strain and 2) the strain is not due to thermal contraction effects but to the sputter deposition itself are made.

A comment on the temperature effects of the stress should be made at this point. Since there is a significant amount of stress in these films, reheating the films to the deposition temperature should relieve only a small portion of the stress in these films.

Compressive stresses of $5.3\pm1x10^9$dyne/cm^2 and $4.8\pm1x10^9$dyne/cm^2 are found at measurement temperatures of 100°C and 24°C respectively in a GdFe film made at -75vdc. Thus thermal contraction effects between the film and the substrate contribute little to the room temperature film stress. The displacement curves for this film are shown in figure 21.

Stripe period studies on films, which have their substrates externally

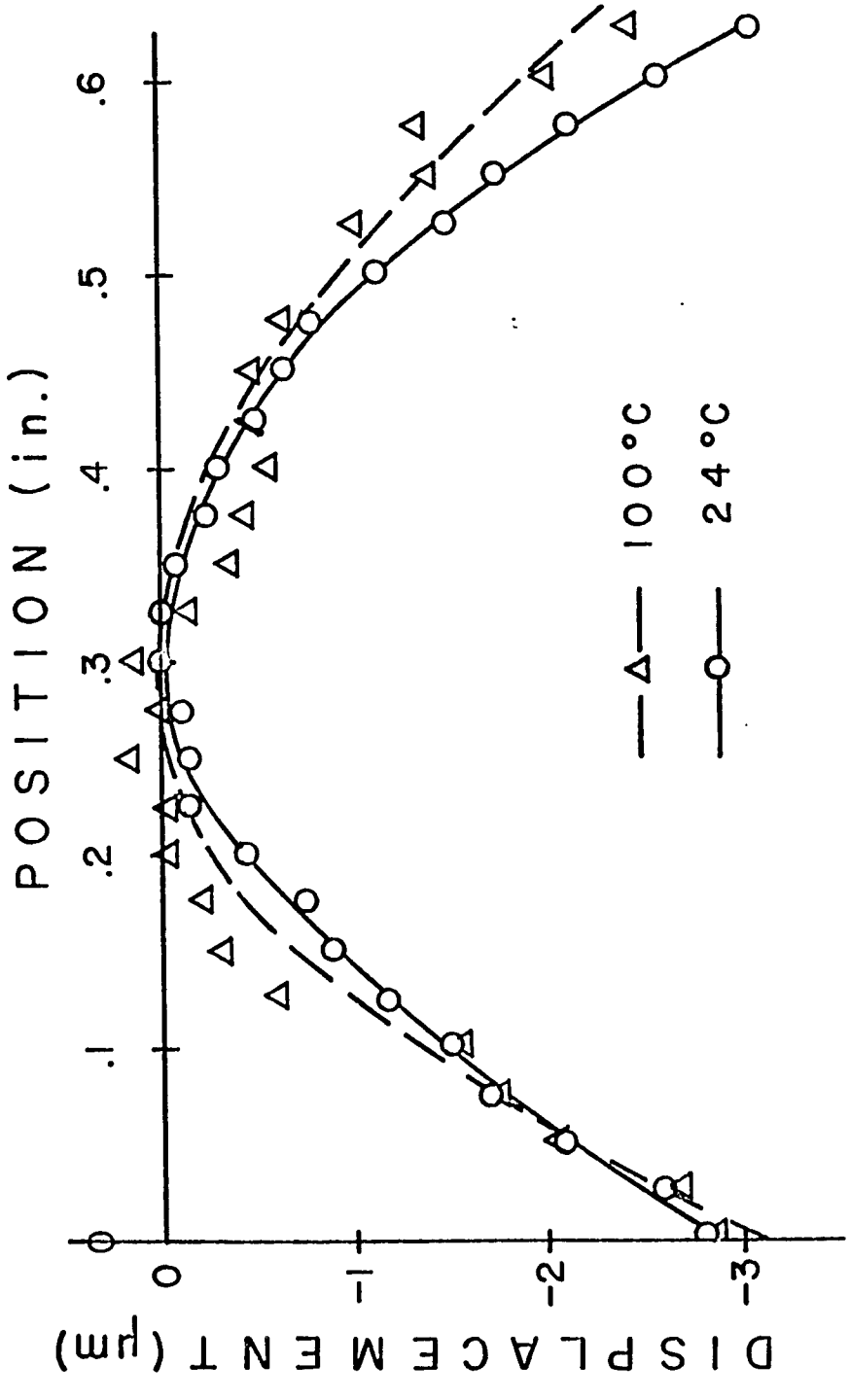

Figure 21: Stress measurement data of a GdFe film. There is little stress relieved by returning the film to its deposition temperature.

stressed to try to relieve the strain, are inconclusive. The tests are inconclusive because the substrates break before any significant film stress can be relieved. The maximum relative change in the stripe periods of the observable stripes is calculated to be about 3% before the substrates break. This value is found by measure the bowing of the glass just at the break pressure; the bowing change is converted to the fractional change in the anisotropy which is related to the fractional change in the characteristic length and then to the fractional change in the stripe period. A maximum fractional change in the stripe period of 3% is unobservable and is the reason for the inconclusiveness of these tests.

If each deposited atom possessed an energy of eV_t, where V_t is the target voltage, it would have to release about 10^{13}erg/cc of energy into the film. Some of this energy will be carried away by the water-cooled substrate. If each backsputtering argon ion gave all of its energy to a single metal atom, each deposited atom would have to release about 10^{15}erg/cc into the film. This value is estimated from the substrate bias voltage, rise in substrate bias current, sample area and deposition rate. The elastic energy density in the films, $E_{elastic}=Xe/2$, is about $3x10^{7}$erg/cc. X is the film stress and e is the strain. The energy of the atoms from the target or the energy of backsputtering ions is much larger than either the elastic or anisotropy energies. Thus from order of magnitude calculations either the target atoms or the substrate bias could cause the anisotropy and stress in these films. This is consistant with the observed effects that 1) the sputter deposition itself is the primary cause of stress in the films and 2) that the wall energy has a bias dependence.

Effects of angle of growth of films upon the easy axis direction is usually attributed to structural growths, such as columnar or longitudinal

growths, as the film is being deposited. This process is seen in evaporated magnetic films [24]. Although columnar growths alone cannot produce sufficient anisotropy for $K_u > 2\pi M_s^2$, the growths can induce strong anisotropic ordering effects. Under certain conditions structural growths might exist in sputtered films. First, growths are favored if the incident atoms from the target are sufficiently unidirectional upon the substrate to cause a pseudo-crystalline coordination with a preferred direction. High deposition rates and sputtering powers enhance this condition. Second, such growths are enhanced by low substrate temperatures because low substrate temperatures inhibit atom migration. Atom migration would break up the preferred growths. High thermal conducting substrates and substrate cooling are important in keeping the film temperature down during sputtering. Thirdly, growths are enhanced if there is insufficient argon damage or film inclusions. Argon damage or film inclusions would tend to break up long range anisotropic growths. Unbiased sputtering or low bias sputtering are preferred for this condition.

Since there is a difference in stripe periods and anisotropy energies observed by Imamura, et. al. and Kobayashi, et. al, with those observed here, the differences may be due to different anisotropy mechanisms and/or to a different level of inverse magnetostrictively induced anisotropy, see figures 13 and 16. In either case, the differences in anisotropy must be due to the differences in the deposition techniques used. The differences in the deposition techniques of Kobayashi, et. al. and Imamura, et. al. and the techniques used here are 1) glass substrates are used here while Kobayashi, et. al. and Imamura, et. al. used silicon wafers, 2) Kobayashi, et. al. used a deposition rate of about 400Å/min while only 30Å/min is used here, 3) dc substrate bias voltages are applied here while no bias

was applied by Kobayashi, et. al. and Imamura, et. al. Argon pressure and substrate bias are shown to effect the wall energies but not to the degree needed to produce the large stripes and anisotropies seen by Kobayashi, et. al. and Imamura, et. al. The conditions which enhance anisotropic structural growths are not only consistant with the sputtered films prepared by Kobayashi, Imamura, and Mimura [22,23,25,26] but also with the co-evaporated films of Orehotsky and Schroeder [3], Taylor [29] and Heiman, et. al. [16]. A deposition rate of 30Å/min is considered to be too low energetically and not sufficiently directional to induce anisotropic structural growths even though it does not cause high film temperatures during deposition. High argon concentrations also may be preventing growths. The deposition temperature of the films made by Kobayashi, et. al. is not high enough to cause high thermally induced stress in the films since silicon wafers were used as substrates.

E) Coercivity and Film Quality:

Films of about the same H_k and $4\pi M_s$ were deposited at 0vdc and -70vdc substrate biases. The coercivity of the films made at 0vdc bias was about 39oe while it was less than 3oe for films made at -70vdc. Low coercivities are also observed for films made at -100vdc and of similar magnetization.

Hysteresis loops taken for films with the same H_k and $4\pi M_s$ but made at -70vdc and 0vdc are shown in figures 22a&b respectively.

In an effort to determine the effect of bias on the quality of the films, a study was made of the film resistivity versus substrate bias voltage, as shown in figure 23. The abrupt drop in resistivity for films made at biases greater than -30vdc indicates that higher backsputtering rates, induced by higher biases, help to produce cleaner films. The similarity between the reduction in coercivity and the reduction in

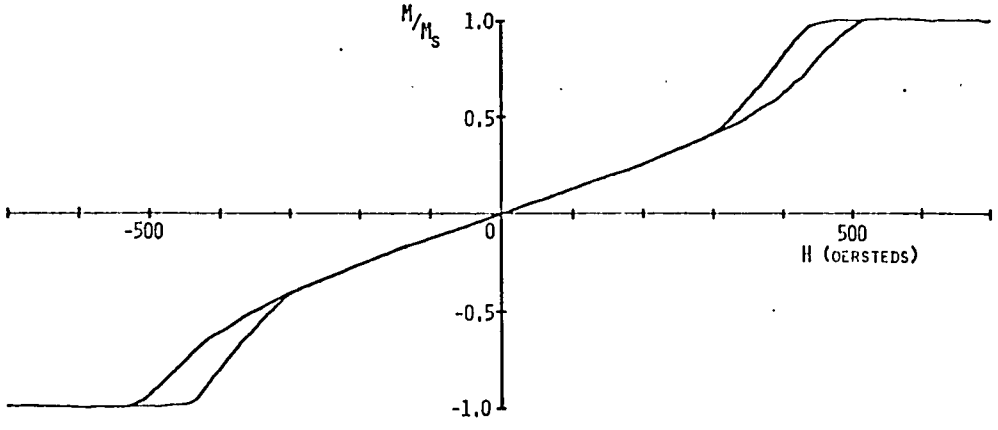

Figure 22a.

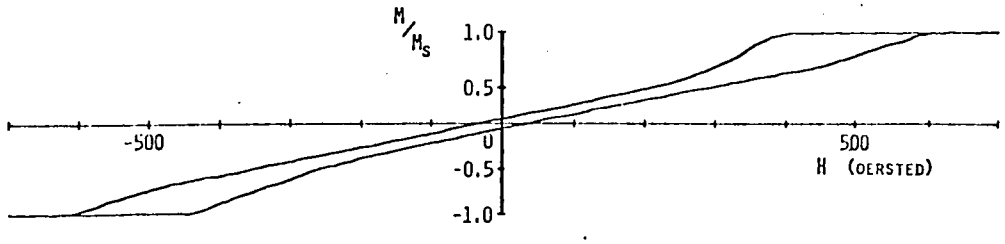

Figure 22b.

Figure 22a&b: Hall hysteresis loops for GdFe films made at (a) -70vdc substrate bias and at (b) 0vdc substrate bias.

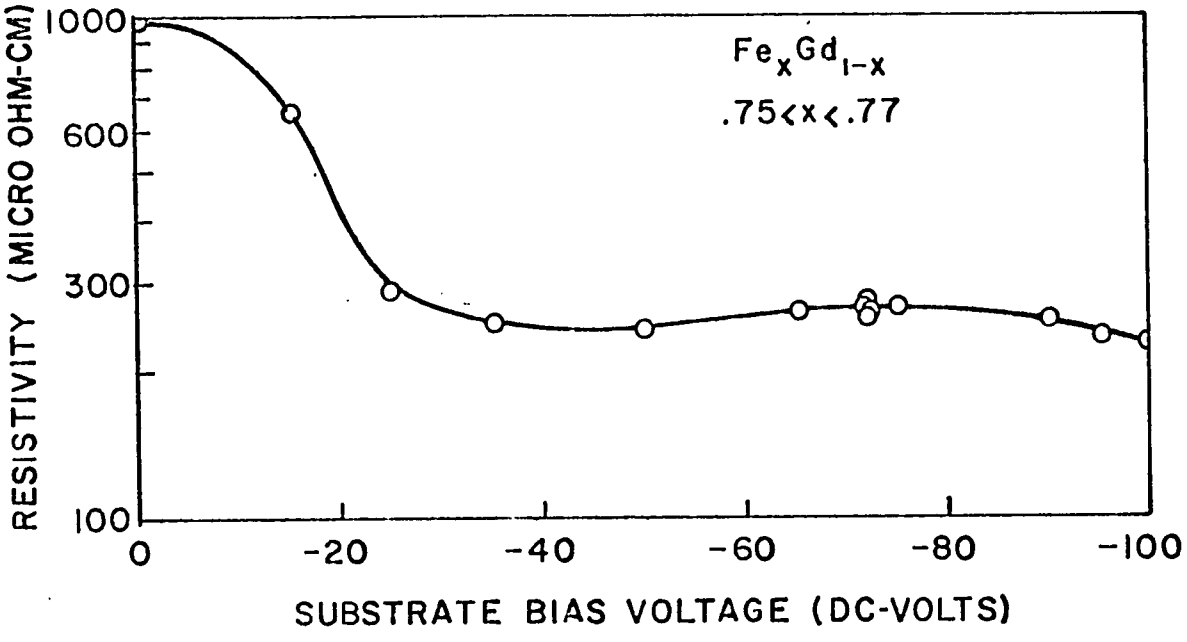

Figure 23: Resistivity dependence on substrate bias: The abrupt drop in the resistivity indicates that only -30vdc bias is needed to produce clean films.

resistivity indicates that cleaner films, which result in a lower resistivity, also give rise to films with better coercive properties.

Films made at less than -30vdc bias show a room temperature compensation composition of about 26 atomic percent gadolinium, in agreement with Imamura, et. al. For higher biased films, the compensation composition is about 24 atomic percent. This shift is probably due to the improved purity of the higher biased films. The compensation composition is determined by reversal of the Hall hysteresis loop [47].

In the discussion of the quality of sputter deposited films, the topic of argon gas inclusions should be included. The argon content of films made here is determined by the method described in the experimental techniques chapter. Argon fractions are investigated in two different experiments: first, argon content versus substrate bias voltage and, second, argon content versus compositon. The uniformity of argon in a film is included in the film uniformity section.

Figure 24 shows the atomic fraction argon versus substrate bias voltage for films with $x=.76\pm.01$, where x is defined by Fe_xGd_{1-x}. Although there is considerable scatter in the data, the scatter can be explained by the possible error margins, which is $\Delta Atm\%A/Atm\%A=.48$ for films with 10Atm%A and x=.76. A 5% uncertainty in the iron counts, a 5% uncertainty in the gadolinium counts and a 5% uncertainty in the thickness determination are the origins of the maximum possible error. A typical error bar is also shown for one of the data points in figure 24. The argon fraction appears to be independent of the substrate bias voltage. Also, no dependence on the sputtering pressure is found. The average argon content is 10.2Atm% which is within the maximum error of most of the data shown. An atomic fraction of .10 argon is quite reasonable when compared with values

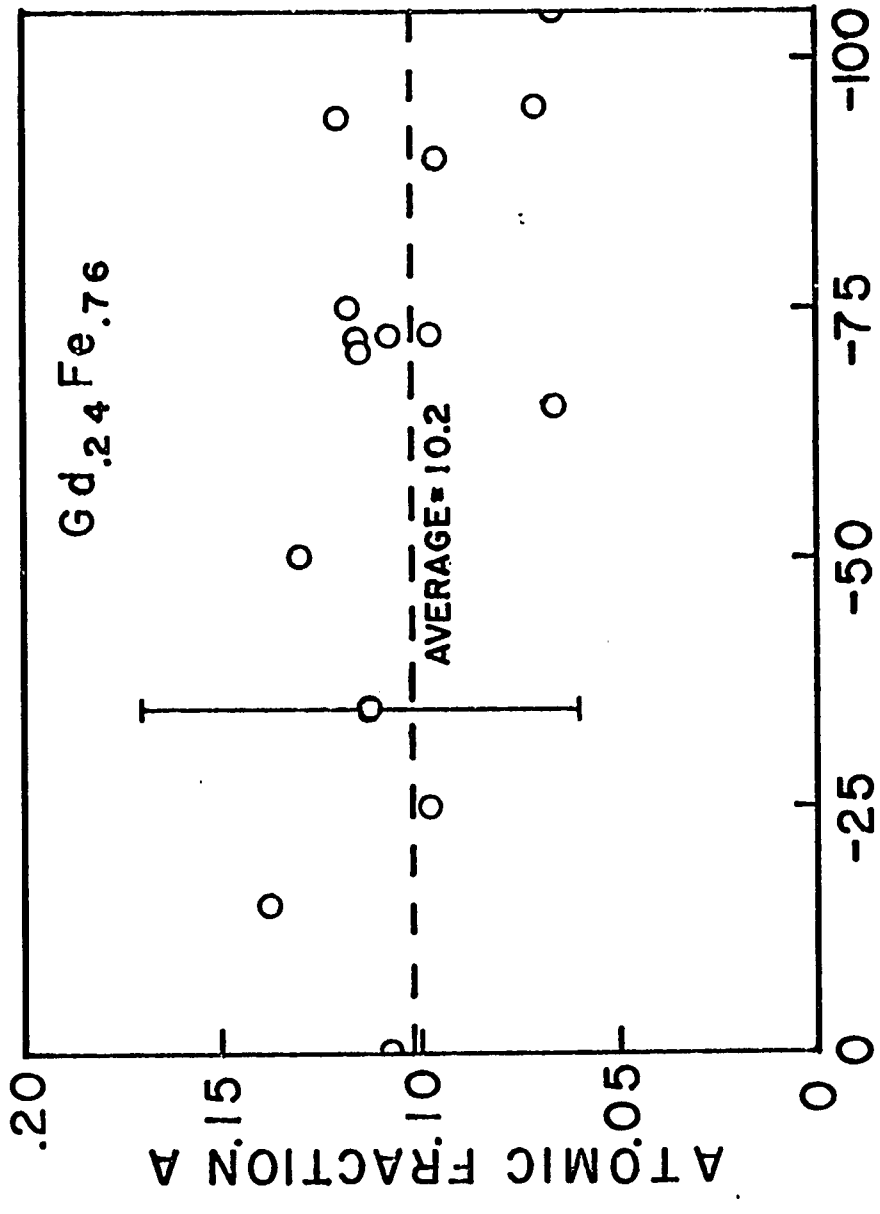

Figure 24: Atomic percent argon in bias sputtered GdFe films with compositions near the compensation composition. There appears to be no trend with substrate bias.

reported in the literature [38,G2] of 7 to 8 Atm%.

An argon fraction of 10.2 Atm% corresponds to 24% argon by volume in films with x=.76. The thickness of each film, assuming that iron and gadolinium are the only constituents, is given as part of the output of composition determination program for Fe_xGd_{1-x} analysis. The difference between the actual thickness, as determined by interferometry, and this x-ray determined effective thickness corresponds to the volume of the film that is assumed to be occupied by argon atoms only. Figure 25 shows the thickness determined by x-ray analysis versus the thickness determined by interferometric means. A fitted curve to the data has a slope of .74 indicating again that about 26% of the film volume is not iron or gadolinium.

The argon content versus conposition of GdFe films deposited with the substrate bias voltage greater than -30vdc are shown in figure 26. The data shows that the argon fraction increases almost linearly with gadolinium fraction to about 66 Atm%Fe, 18 Atm%Gd, and 16 Atm%A. This limit corresponds to x=.79 for Fe_xGd_{1-x}. Beyond the limit, the argon fractions appear to be somewhat constant at about 16 Atm%A.

Using x-ray fluorescence data taken on a microprobe, the compositional uniformity of the Gd-Fe films can be investigated. The Fe_xGd_{1-x} and the FeGdA composition analysis programs used in the data reduction are described in the experimental techniques chapter. The GdFe film studied was deposited at -94vdc and at 10um of argon pressure. The film has an average x=.757 with a maximum deviation of .014, see figure 27a. This average is in excellent agreement with the composition found by x-ray fluorescence data taken on a GE XRD-5 fluorscent analysis spectrometer, the composition found by this technique was x=.75. The part of the film near the holder center is slightly higher in iron, as determined by the microprobe. This indicates

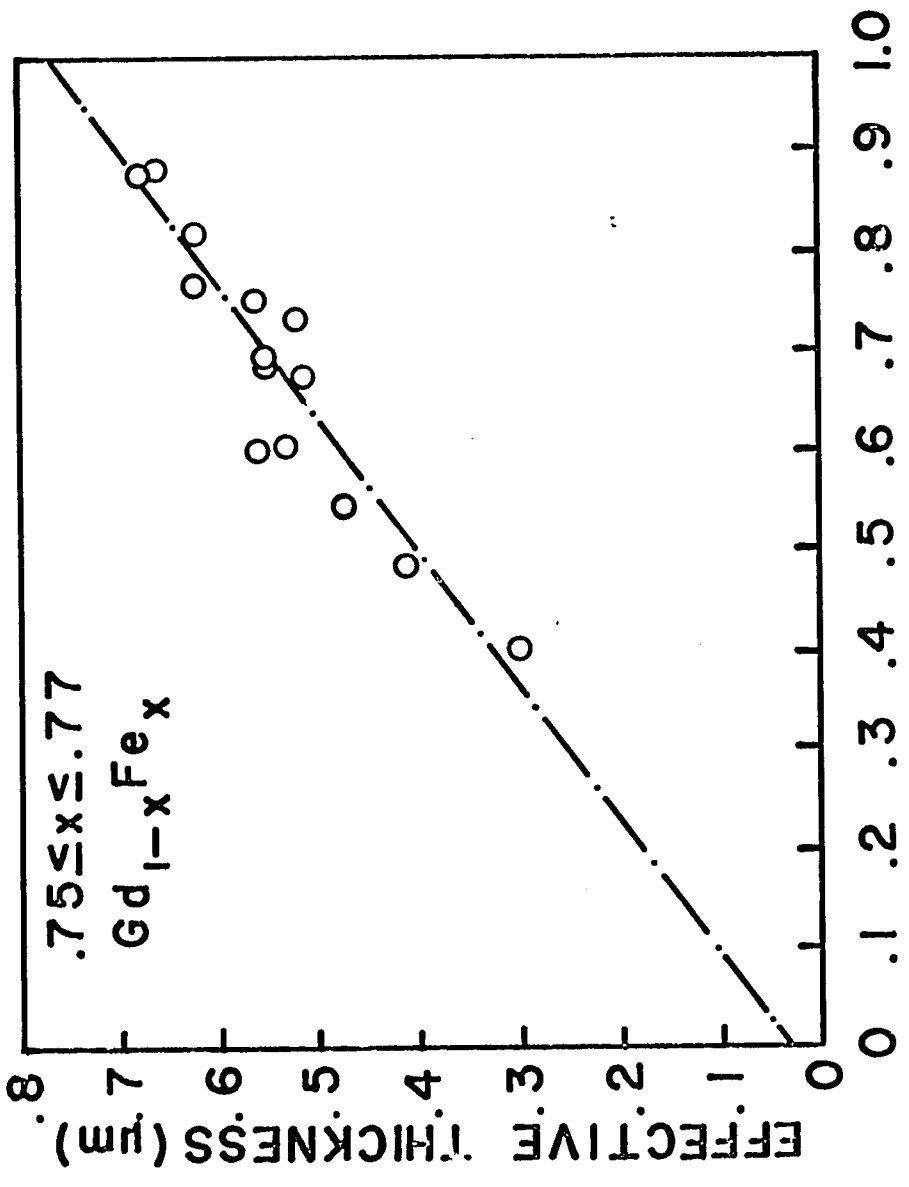

Figure 25: Comparison of the actual thickness observed by interferometric techniques with the effective thickness of just the Gd and the Fe atoms counted by x-ray fluorescence.

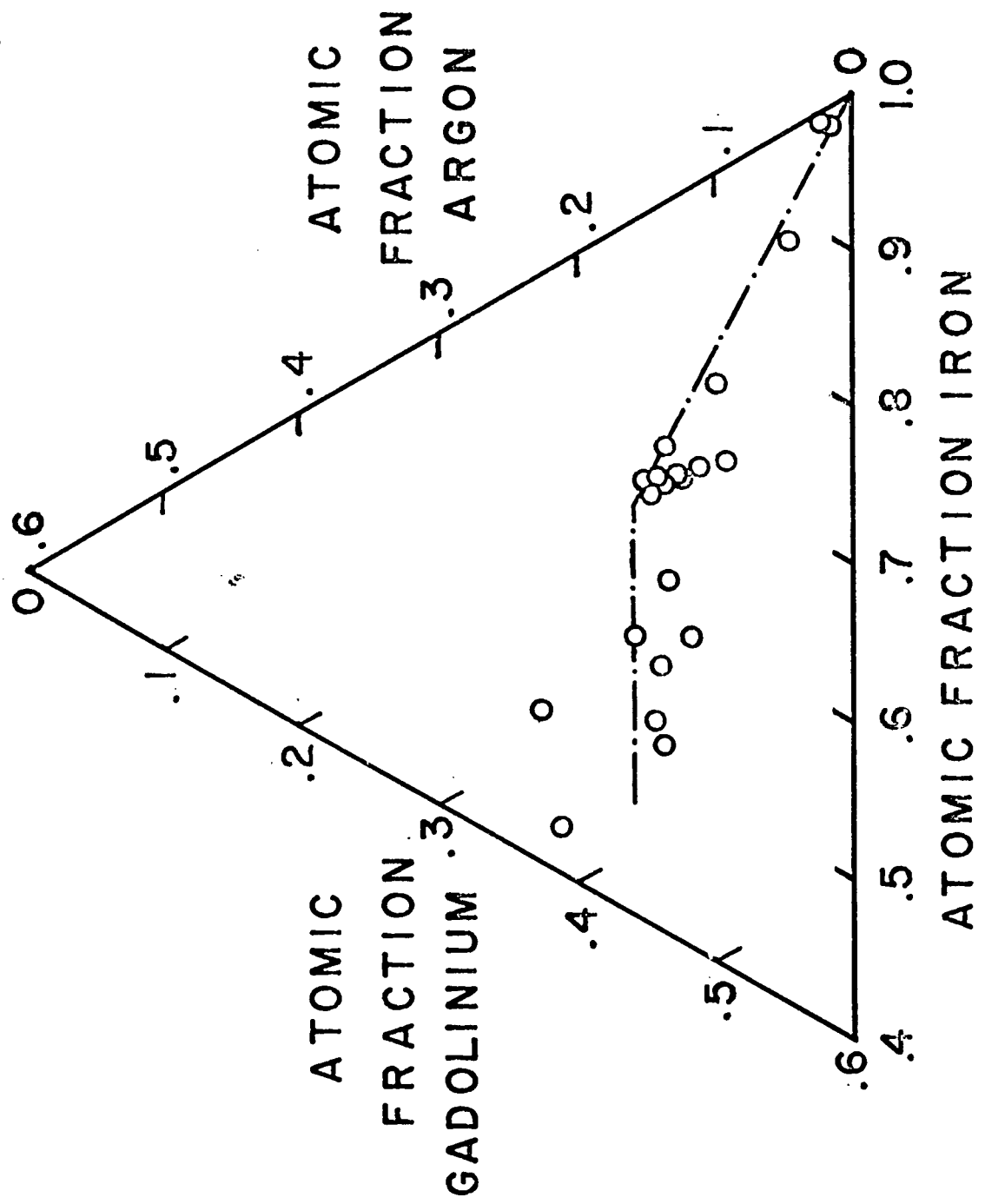

Figure 26: Composition of GdFeA bias sputtered films.

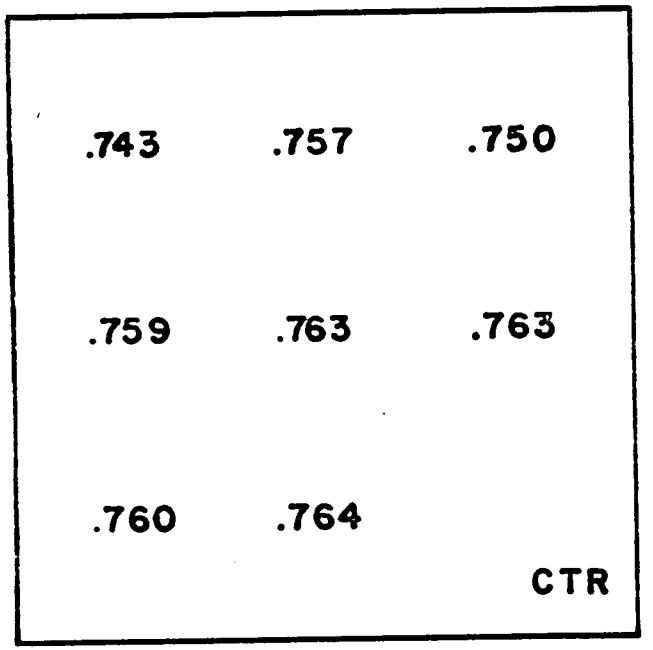

Figure 27a.

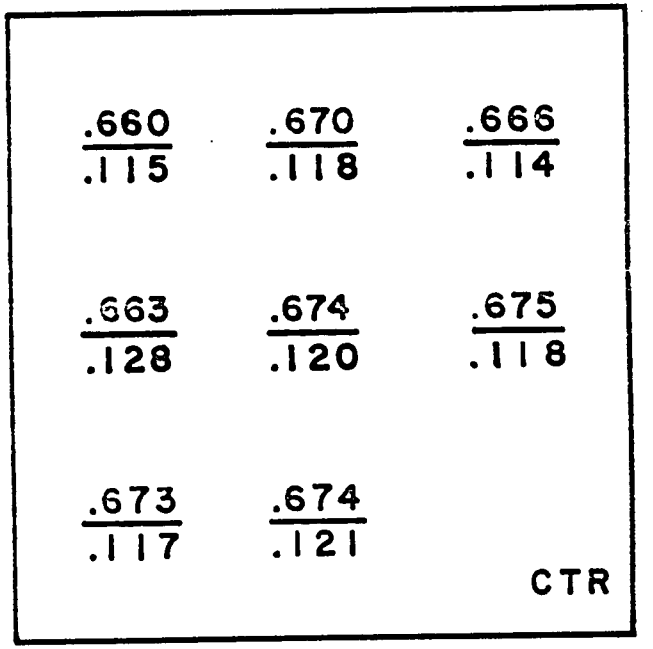

Figure 27b.

Figure 27a&b: Uniformity tests on a GdFe film: (a) x for $Gd_{1-x}Fe_x$ and (b) $\frac{x(1-y)}{x}$ for $(Fe_xGd_{1-x})_{1-y}A_y$

that more gadolinium is backsputtered near the center of the substrate holder than at the edges. The film has the Atm%Fe and the Atm%A shown in figure 27b. No trend in the argon fraction can be seen in figure 27b but, again, an iron richness is observed for the part of the film nearest the center of the holder.

The presence of argon is confirmed directly by using the microprobe in the x-ray fluorescence mode on the K_α line of argon. The actual number of counts taken was about five times the backround counts taken on the argon line. An argon standard, which is not available for this work, is needed to obtain quantitative data by this means.

F) Magnetization and Moment Properties:

The magnetization and moment properties will be discussed in this section, first, from the point of view of assuming that argon is not in the films and, second, from the point of view of including argon in the magnetization calculations. A comparison of these two approaches will give the importance of argon considerations when evaluating the magnetization and moment properties of GdFe bias sputtered films.

1) Argon not included:

The magnetization of sputtered $Gd_{1-x}Fe_x$ films with compositions between 55 Atm%Fe and 99 Atm%Fe are shown in figure 28. The films studied were made with substrate bias voltages greater than -30vdc. The thickness of these films was determined by interferometry and the magnetic moments of the films were measured for the center one centimeter diameter of the films. The remainder of the film was removed by etching in dilute HNO_3. An inductive M-H loop tracer was used to determine the moments of these films while the reversal of the Hall hysteresis loop was used to determine the room temperature compensation composition. Although the magnetization

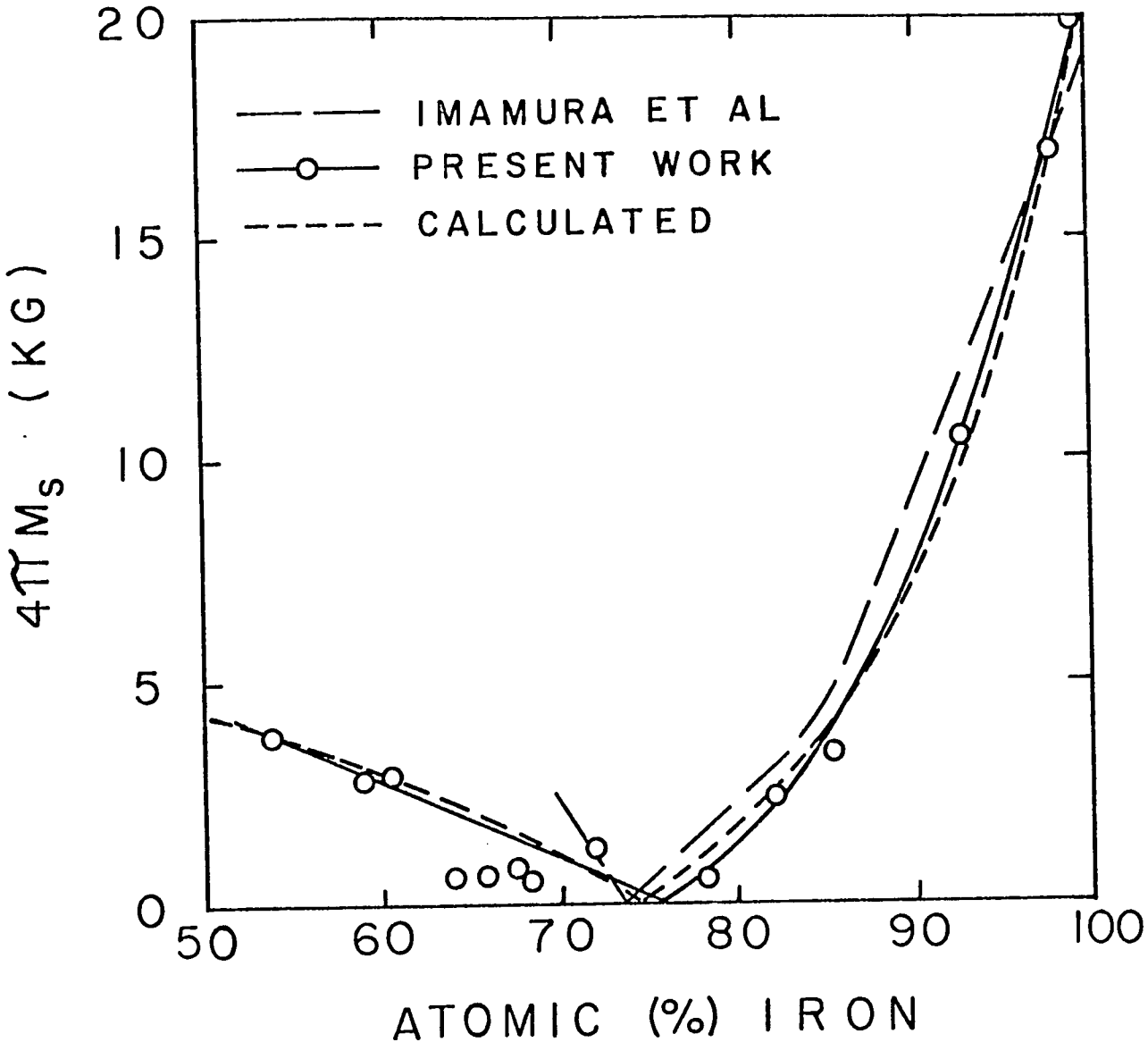

Figure 28: Magnetization dependence on composition: Note that the data is very close to that observed by Imamura, et. al. [23].

data varies smoothly with x, the scatter should be noticed. The magnetization data presented in figure 28 and the magnetization curve of Imamura, et. al. show a rapid drop with increasing Gd additions to about 15 Atm% gadolinium, $\Delta(4\pi M_s)/\Delta x$=1.3KG/Atm%. For gadolinium fractions greater than 15 Atm% the magnetization curves show less dependence on composition, $\Delta(4\pi M_s)/\Delta x$=.3KG/Atm%. To accommodate such a low magnetization dependence on composition for films near the room temperature compensation composition, the iron moment, u_{fe}, must be about $1.3u_b$ and the exchange integrals about $J_{fefe}>2.4\times10^{-14}$erg, $J_{fegd}=J_{gdfe}=-1.4\pm.2\times10^{-15}$erg and $J_{gdgd}=1.2\pm.2\times10^{-16}$erg (see appendix for the magnetization calculation program.)

Figure 28 also shows the room temperature magnetization versus composition curve found by using the exchange integrals given above for $.5< x <.85$ and higher J_{fefe} for $x > .85$. For the calculated curve $u_{fe}=1.3u_b$ for $.5< x <.85$ and

$$u_{fe}(x)=2.2u_b - (2.2u_b-1.3u_b)\cdot(1-x)/.15$$

for $x > .85$. The iron moment $u_{fe}(x)$ for $x > .85$ is an assumed linear moment reduction with increasing atomic fraction Gd. Such a Fe moment reduction with composition and antiferromagnetic coupling of the Gd moments to the Fe moments is needed to explain the rapid magnetization drop with increasing Gd additions. No iron moment changes versus composition are made for the magnetizations calculated in the composition range of $.5< x <.85$ even though small fluctuations have been observed for the crystalline alloys in this range [48,49]. The calculated magnetization curve closely fits both the experimental data presented and the curve representing the magnetization data of Imamura, et. al. The calculated magnetization curve is fitted by observation only and not by a least-

squares type of fit.

In GdFe sputtered films with up to 15 Atm%Gd the iron moment rapidly decreases with increasing Gd concentrations due the charge transfer [10] and there may be a lowering of the iron-iron exchange integral with increasing Gd additions. In the composition range $.5< x <.85$, the iron moment value is about $1.3u_b$ and the magnetization can be adequately described by exchange integrals that do not change throughout this range.

2) Argon considered:

The effect of argon is assumed to be dilution only and not to effect the iron moment through electron transfer as has been used in calculating the magnetic properties of GdCoMo films [50]. The magnetization calculation program accounts for the effects of argon by altering the density. Altering the density, in turn, effects the calculated magnetization through two mechanisms, 1) reducing the moment density and 2) reducing the molecular field constants by altering the number of nearest neighbor moments.

Fitting the magnetization versus composition data for $(Fe_xGd_{1-x})_{1-y}A_y$ gives:

$$u_{fe}=1.5u_b \qquad \text{for } .5< x <.85$$

$$u_{fe}=2.2u_b - (2.2u_b-1.5u_b)\cdot(1-x)/.15 \qquad \text{for } x >.85$$

$$J_{fefe}>1.2x10^{-14}\text{erg}$$

$$J_{fegd}=-1.8x10^{-15}\text{erg}$$

$$J_{gdgd}=1.2x10^{-16}\text{erg}$$

for argon fractions, y, of

$$y=8/9 \text{ (Atomic fraction Gd)}=8/9\cdot(1-x)\cdot(1-y) \qquad \text{for } x >.85$$

$y=.16$ for $.5 < x < .85$

These compositions are represented by the dashed line in figure 26 in the argon fraction discussion. In the compensation composition region, the estimated errors are: $.05u_b$ for u_{fe}, $0.2x10^{-15}$erg for J_{gdfe} and $0.2x10^{-16}$erg for J_{gdgd}. The calculated curve is plotted in figure 29. Including argon in the calculation of the magnetization versus composition curve gives a significantly different value for the iron moment. With argon considered $u_{fe}=1.5u_b$ which is closer to the observed iron moment of $1.6u_b$ for the crystalline alloy with $x=.75$ [49] than the $1.3u_b$ calculated without considering argon in the films.

G) Exchange Stiffness and Discussion:

This section concerns only the films with compositions near the room temperature compensation composition.

The importance of the exchange constant of a bubble material is discussed by Kryder, et. al. [11] and Chaudhari, et. al. [17]. The exchange constant calculated by Hasegawa [6] is about $6x10^{-7}$erg/cm for GdCo sputtered films with compositions near the compensation composition. However, no experimental determination of the exchange constant can be found in the literature for comparison with this calculation.

For the evaluation of the exchange constant of the GdFe films made here, two approaches are used. In the first approach, the exchange stiffness is determined indirectly through experimental results, while by the second approach, is calculated from the room temperature magnetization data using the exchange constant equation of Hasegawa [6]. Exchange constant calculations which both include and omit argon effects are presented.

1) Experimentally indirect approach:

Since the composition ranges of observable and low coercivity stripes

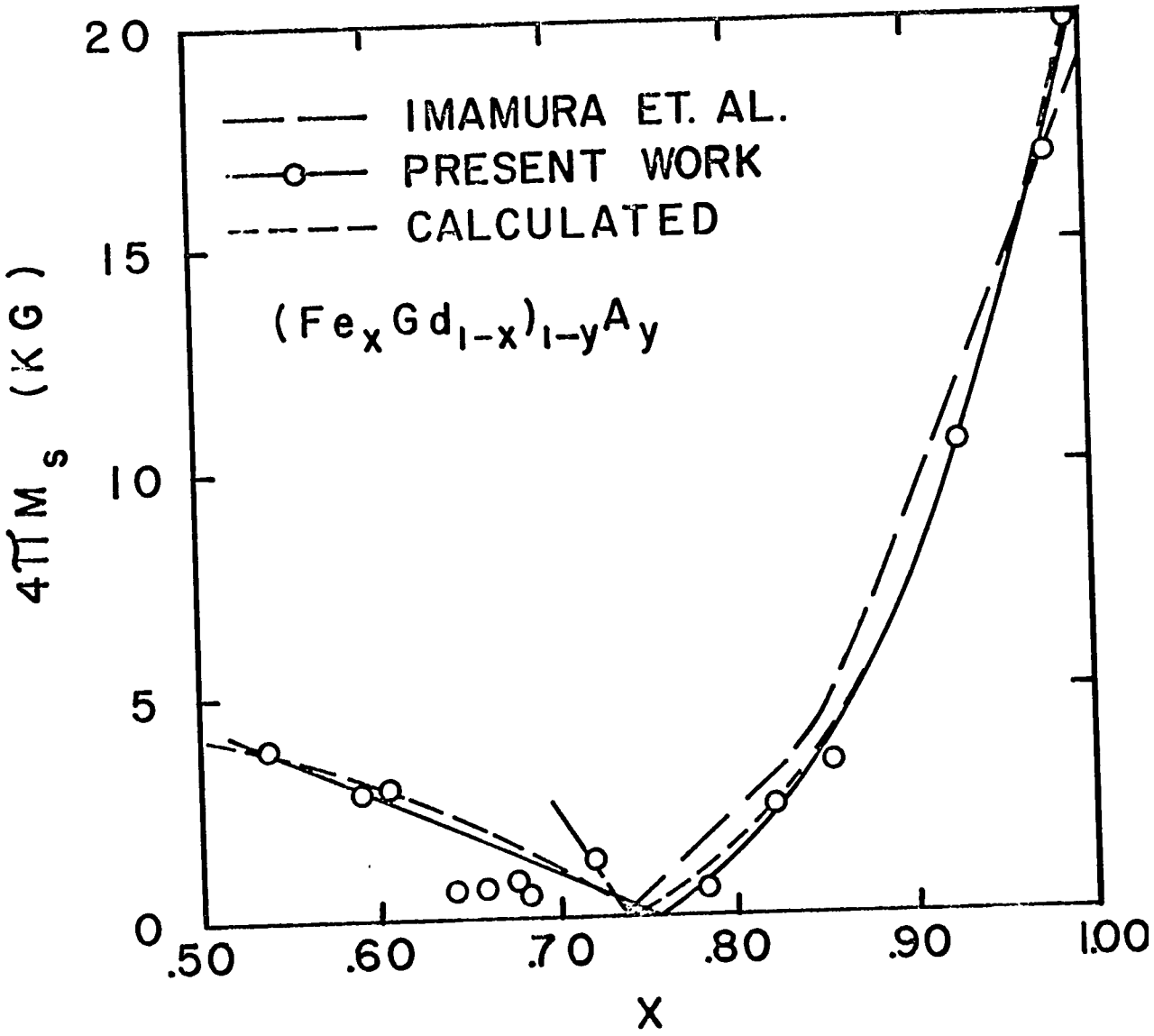

Figure 29: Same as Figure 28 except that argon effects are included in the magnetization calculations.

is about 1.5 Atm% wide on each side of the compensation composition, the exchange stiffness, A, is expected to vary little through these ranges. For the wall energy, $\sigma=4\sqrt{AK_u}$, of a material to remain constant throughout a composition range where the exchange stiffness varies little, the anisotropy energy of the material should also vary little. However, the anisotropy energy is not constant for these films as is seen in figure 16, but the wall energy of each film and its corresponding anisotropy can provide a consistancy check on the exchange stiffness. For the consistency check, σ^2 versus K_u is plotted for the samples for which both σ and K_u are known. σ^2 versus K_u is shown in figure 30. The slope of the fitted curve to this data gives an exchange constant of 1.82×10^{-7}erg/cm. An exchange constant of 1.82×10^{-7}erg/cm is about one-third of the exchange stiffness calculated for GdCo amorphous films [6]. Although there is considerable scatter in the data presented there are also large error margins to explain the scatter. The large error margins are primarly due to a 10 percent uncertainty in the magnetization. A ten percent error in the magnetization contributes a 40% uncertainty in σ^2 and about a 10% uncertainty in K_u. Carlo, et. al. [51] report 18% possible error in the calculation of the exchange constant for garnet materials using characteristic length, magnetization and anisotropy data. For the films examined here, 40% possible error is a reasonable estimate. Since the data of figure 30 shows a linear dependence of σ^2 on K_u, the exchange stiffness is essentially a constant and not dependent on K_u throughout this composition range. If A varied as $1/K_u$ then σ^2 would be the same for all values of K_u.

Figure 30 shows that there is a 50% standard deviation in the exchange stiffness constants calculated from the wall energies and anisotropies

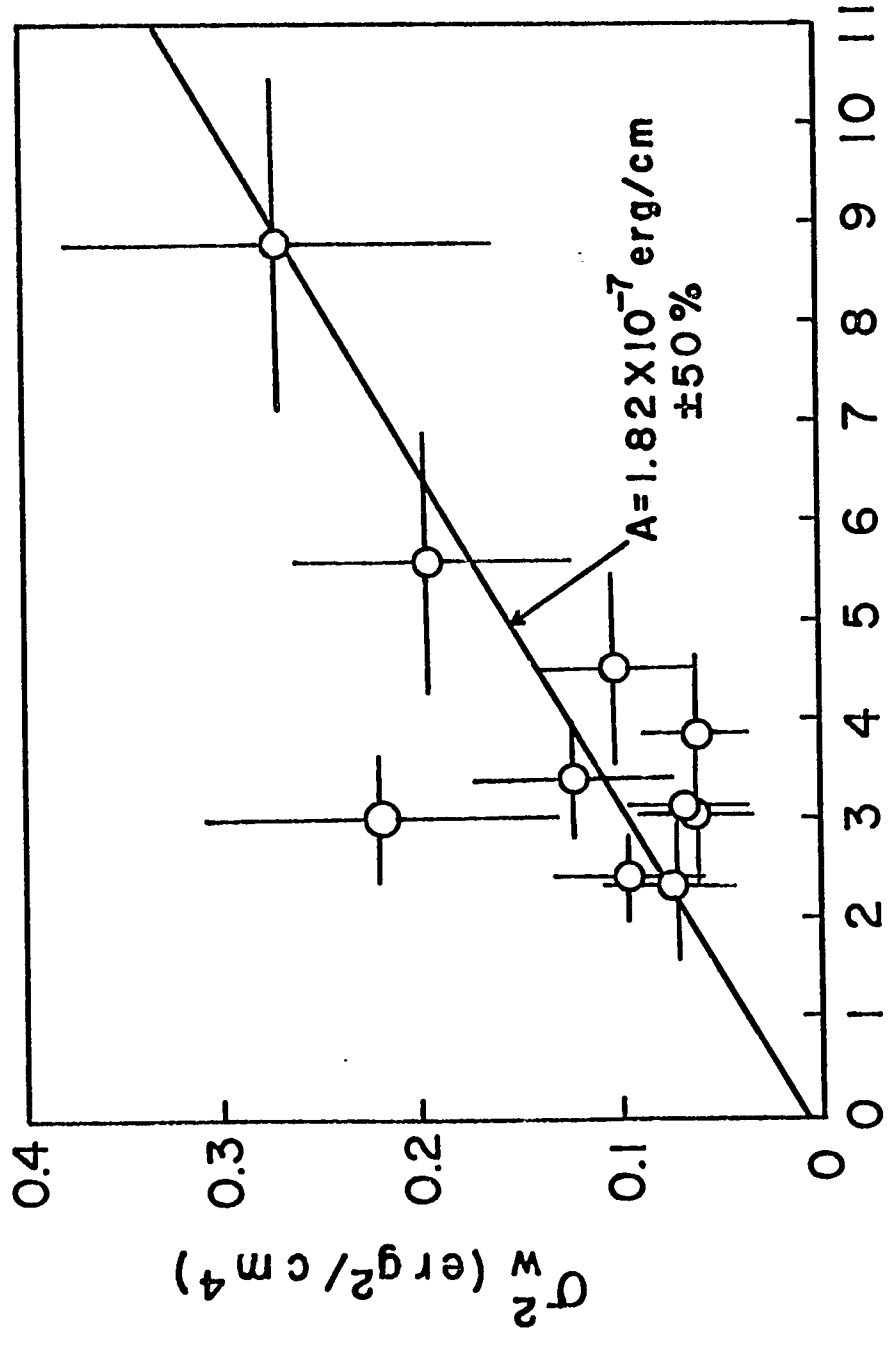

Figure 30: Wall energy squared versus anisotropy energy: There is scatter in the exchange data; this could indicate that there are fluctuations in the ordering length.

for each film, There may be an actual scatter in the exchange constants of these films since the maximum possible measurement error is estimated to be 40%. An actual scatter in the exchange constants can be explained by different ordering lengths. Bias sputtered films which contain large amounts of argon may be considered to have only isotropic short range ordering; not the longer range ordering of pseudo-crystalline growths postulated for the evaporated films [16]. Scatter in the ordering lengths would effect the room temperature magnetization if it effects the exchange interactions. Fluctuations in the exchange constant have been related to the cause of the coercivity in sputtered GdCo films [14]. The scatter in the magnetization data presented in figure 29 and the scatter in the data of Orehotsky and Schroeder [3], Chaudhari, et. al. [21] and Taylor [29] could be explained by different ordering lengths.

Since the films made at Ovdc bias had enough impurities to effect the resistivity and the coercivity, they are not used in evaluating the exchange properties of these GdFe films because of the unknown effect of these type of impurities in the exchange properties.

2) Calculated:

i) Without argon considered:

Using the exchange integrals and the moments found for the calculated magnetization curve without argon effects taken into account, a minimum exchange constant of 4.7×10^{-7} erg/cm is found for Fe_xGd_{1-x} films with compositions near the compensation composition from the equation given by Hasegawa [6] for the exchange constant.

$$A = n_{fefe} J_{fefe} \bar{S}_{fe}^2 x^2 / a_{fefe} + (n_{fegd} + n_{gdfe}) |J_{fegd}| \bar{S}_{fe} \bar{S}_{gd} x(1-x)/a_{fegd} + n_{gdgd} J_{gdgd} \bar{S}_{gd}^2 (1-x)^2 / a_{gdgd} \qquad \text{eq. 3}$$

where n_{ij} is the number of pairs per unit volume (n=2 is used here), $\bar{S}_i$ is the 300°K spin value and x^2,$x(1-x)$ and $(1-x)^2$ are the probabilities of finding the atom pairs FeFe, FeGd, and GdGd respectively. The atomic spacings used are: a_{fefe}=2.5Å, a_{fegd}=3Å, a_{gdgd}=3.5Å [28] and S_{gd}=3.5 and $g_{fe}=g_{gd}$=2 are used here.

ii) With argon considered:

The exchange constant will be recalculated but this time argon effects will be considered. Even though argon has been reported in sputtered GdCo films [38], is has not been taken account in the calculation of the exchange constant, the exchange integrals or the transition metal moments for sputtered GdCo and GdCoX films [7,50,52].

Using the exchange integrals and moments found from the magnetization calculations with argon effects considered, a minimum exchange constant of A=2.5x10^{-7}erg/cm is found. This value is calculated using an altered form of equation 3. The altered exchange constant equation takes account of the reduced concentration of the moments by the $(1-y)^2$ terms; the equation is:

$$A=n_{fefe}J_{fefe}\bar{S}_{fe}^2x^2(1-y)^2/a_{fefe} + (n_{fegd}+n_{gdfe})|J_{gdfe}|\bar{S}_{fe}\bar{S}_{gd}x(1-x)(1-y)^2/a_{fegd} + n_{gdgd}J_{gdgd}\bar{S}_{gd}^2(1-x)^2(1-y)^2/a_{gdgd} \quad \text{eq. 4}$$

3) Comparison:

A comparison of the exchange constant values found experimentally, 1.8±.9x10^{-7}erg/cm and the calculated minima of 4.7x10^{-7}erg/cm and 2.5x10^{-7}erg/cm show that the argon content must be considered in the exchange constant and magnetization calculations. This is consistant with the importance of the argon fraction found in calculating the moment values of the iron atoms. The average exchange constant found experimentally

is considered acceptable when compared with the calculated minimum value of 2.5×10^{-7} erg/cm which is found by accounting for the argon effects in the films.

Valuable information about the exchange constant, moment, and magnetization trends with composition can be found from examining equation 4. The exchange constant, A, is dependent both upon the average moments of the Gd and the Fe atoms and the concentrations of GdGd, GdFe and FeFe atom pairs. For GdFe films of about x=.75 the first term of equation 4 is the major contributor to the exchange constant at room temperature. There are several reasons for this: 1) there is a high atomic fraction at these compositions, 2) the 300°K iron moment, $\bar{u}_{fe}$, is about equal to the iron moment at 0°K, u_{fe}, 3) the iron-iron exchange integral is about 10 times the iron-gadolinium exchange integral and about 100 times the gadolinium-gadolinium exchange integral and 4) the 300°K Gd moment, $\bar{u}_{gd}$, is about one half of the gadolinium 0°K moment, u_{gd}. Further examination of the exchange equation gives information about the magnetization dependence in these films. Since the 300°K iron moment is about equal to the 0°K iron moment for x=.75, the change in the magnetization versus composition is due predominately to 1) the increasing concentration of gadolinium moments coupling antiferromagnetically to a decreasing concentration of Fe moments for increasing Gd additions, 2) the reduction of the 300°K Gd moment value with increasing Gd concentrations.

CHAPTER V: CONCLUSIONS

The static magnetic properties of dc bias sputtered GdFe amorphous films are summarized in this chapter and the results are used to evaluate GdFe films for bubble material purposes.

Gadolinium-iron films deposited by dc biased rf sputtering are found to have the following properties:

1) They have smaller stripe periods, wall energies and anisotropies than unbiased sputtered or evaporated GdFe films of similar magnetization.

2) They have wall energies nearly independent of magnetization but dependent upon the substrate bias used for the films near the compensation composition.

3) The normal anisotropy is predominantly stress induced; i.e., the anisotropy mechanism is inverse magnetostriction. The stress is not caused by thermal contraction effects between the film and the substrate but by the sputter deposition process itself. There appears to be little dependence of anisotropy on bias sputtering voltage for films with $x \simeq .75$.

4) The magnetization dependence on composition agrees with the data of Imamura, et. al. There also appears to be considerable scatter in the data itself. A two sublattice ferrimagnetic model is used to find the moment and the exchange integral properties of these films. The iron moment, for $x \simeq .75$, is about $1.5u_b$ consistant with bulk GdFe. The reduced moment indicates charge transfer to the iron atom from the gadolinium atom. Argon inclusion effects must be included in the magnetization calculations in order to give a reasonable iron moment value. There are two major causes of magnetization change with composition, first, the change in the concentration of iron and gadolinium moments and, second, the change of the room temperature gadolinium moment value.

5) The exchange constant is about $1.8\pm.9\times10^{-7}$erg/cm for $x\simeq.75$ which agrees well with the minimum calculated value of 2.5×10^{-7}erg/cm. Argon effects must be included in the exchange calculations also to give consistant results. The exchange constant is dominated by the iron-iron moment coupling term of the high concentration of iron atoms and a high iron-iron moment exchange integral.

6) The coercivity is low for films made with substrate bias voltages greater than -30vdc. Below -30vdc, the high coercivities observed are impurity induced.

7) The films are suspected to have short range isotropic ordering. However, fluctuations in the ordering length may alter the exchange constant values and the room temperature magnetization values.

The magnetic properties which are advantageous for using bias sputtered GdFe films as a magnetic bubble material are the following:

1) Bias sputtering GdFe films can be made with the low magnetizations, proper anisotropies, wall energies, exchange constants and coercivities for a good bubble material.

2) The wall energy can be adjusted by choosing the proper substrate bias voltage during the deposition.

3) The wall energy is nearly independent of magnetization.

Bias sputtered GdFe films have some properties that are undesirable in a bubble material. They are the following:

1) The anisotropy is stress induced. It can be destroyed by relieving the stress in the films.

2) The magnetization is heavily dependent upon composition for films near the compensation composition. This may make the repeated fabrication of useable bubble material too heavily dependent upon composition control

to be practical.

3) There is considerable scatter in the magnetization data. This scatter also makes the repeated fabrication of good bubble material difficult. This scatter can be attributed to fluctuations in the materials ordering lengths.

REFERENCES:

1. A. A. Thiele, "Energy and general translation force of cylindrical magnetic domains", Bell Syst. Tech. J., 50, pg. 711-773, 1971.

2. A. H. Bobeck, "Properties and device applications of magnetic domains in orthoferrites," Bell Syst. Tech. J., 46, no. 8, Oct. 1967, pg. 1901.

3. J. Orehotsky and K. Schroeder, "Magnetic properties of amorphous $Fe_y Gd_x$ alloy thin films," J. A. P., vol. 43, pp. 2413-2417, 1972.

4. P. Chaudhari, J. J. Cuomo, R. J. Gambino, "Amorphous metallic films for bubble domain applications," IBM J. of Res. and Dev., 17, pg. 66-68, 1973.

5. D. C. Cronemeyer, "Perpendicular anisotropy in $Gd_{1-x}Co_x$ amorphous films prepared by rf sputtering," 19th Conference on Magnetism and Magnetic Materials, Boston, Mass., Nov. 1973.

6. R. Hasegawa, "Static bubble domain properties of amorphous GdCo films," J. A. P., 45, 7, pp. 3109-3112, July 1974.

7. H. C. Bourne, Jr., R. B. Goldfarb, W. L. Wilson, Jr., and R. Zwingman, "Effects of dc bias on the fabrication of amorphous GdCo rf sputtered films," IEEE Mag. Trans., Vol. 11, No. 5, pp. 1332-1334, Sept. 1975.

8. R. W. Shaw, R. M. Sanfort and J. W. Moody, "Characterization techniques study report," Report No. MRC-SL-339, Advanced Research Project Agency, Washington D.C., July 1972.

9. K. Okamoto, T. Shirakawa, S. Matsushita, and Y. Sakuri, "Hall effect in GdCo sputtered films," INTERMAG Conf., Toronto, Canada, April 1974.

10. L. J. Tao, S. Kirkpatrick, R. J. Gambino amd J. J. Cuomo, "Charge transfer and magnetic properties of amorphous $Gd_{.33}Co_{.67}$", Solid State Communications, Vol. 13, pp. 1491-1494, 1973.

11. M. H. Kryder, K. Y. Ahn, G. S, Almasi, G. E. Keefe, and J. V. Powers, "Bubble to T-I bar coupling in amorphous film small bubble devices", INTERMAG Conf., Toronto, Canada, April 1974.

12. K. Y. Ahn, T. H. P. Chang, M. Hatzakis, M. H. Kryder, and H. Luhn, "Electron beam fabrication of high-density amorphous bubble film devices", IEEE Mag. Trans., Vol. 11, No. 5, pg. 1142, Sept. 1975.

13. M. H. Kryder, K. Y. Ahn and J. V. Powers, "Amorphous film magnetic bubble domain devices," IEEE Mag. Trans. Vol. 11, No. 5, Pg 1145, Sept. 1975.

14. R. Hasegawa, R. J. Gambino, J. J. Cuomo and J. F. Ziegler, "Effect of thermal annealing and ion radiation on the coercivity of amorphous GdCo films", J. A. P., Vol. 45, No. 9, pg. 4036, Sept. 1974.

15. R. J. Gambino, J. Ziegler, and J. J. Cuomo, "Effects of ion radiation damage on the magnetic domain structure of amorphous GdCo alloys", App. Phys. Lett., Vol. 24, No. 2, Pg. 99, Jan 15, 1974.

16. N. Heiman, A. Onton, D. F. Kyser, K. Lee, and C. R. Guarnieri, "Uniaxial anisotropy in rare earth (Gd, Ho, Tb)- transition metal (Fe, Co) amorphous films", 20th Conference on Magnetism and Magnetic Materials, San Francisco, Calif., Dec. 1974.

17. P. Chaudhari, J. J. Cuomo, R. J. Gambino, S. Kirkpatrick, and L. J. Tao, "Ternary amorphous alloys for bubble domain applications," 20th Conf. on Magnetism and Magnetic Materials, San Francisco, Calif., Dec. 1974.

18. R. Hasegawa, B. E. Argyle, L. J. Tao, "Temperature dependence of magnetization in amorphous GdCoMo films," 20th Conf. on Magnetism and magnetic materials, San Francisco, Calif., Dec. 1974.

19. R. J. Kobliska and A. Gangulee, Annealing behavior of amorphous GdCoMo thin films," 20th Conf. on Magnetism and Magnetic Materials, San Francisco, Calif. Dec. 1974.

20. P. Chaudhari and D. C. Cronemeyer, "The temperature dependence of the uniaxial anisotropy of $Gd_{1-x-y}Co_xMo_y$ amorphous alloy films on glass substrates," 21st Conference on Magnetism and Magnetic Materials, Philadelphia, Pa., Dec. 1975.

21. P. Chaudhari, J. J. Cuomo, R. J. Gambino, "Amorphous films for magnetic bubble and magneto-optic applications" 19th conference on Magnetism and Magnetic Materials, Boston, Mass., Nov. 1973.

22. T. Kobayashi, N. Imamura, Y. Mimura, "Magnetic properties of GdFe amorphous alloy films prepared by sputtering," 20th Conf. on Magnetism and Magnetic Materials, San Francisco, Dec. 1974.

23. N. Imamura, Y. Mimura, and T. Kobayashi, "Amorphous GdFe alloy films prepared by rf co-sputtering technique," 7th International Conference on Magnetic Films, Regensburg, Germany, April 1975.

24. D. O. Smith, M. S. Cohen, and G. P. Weiss, "Oblique incidence anisotropy in evaporated permalloy films", J. A. P., Vol. 31, No. 10 pp. 1755-1762.

25. Y. Mimura, N. Imamura and T. Kobayashi, "Preparation and some magnetic properties of amorphous Gd_xFe_{1-x} alloy thin films", J. A. P., Vol. 47, No. 1, Pg. 368, Jan. 1976.

26. N. Imamura, Y. Mimura, T. Kobayashi, "Spark like domain pattern and hysteresis loops of amorphous Gd-Fe alloy films", Applied Phys. Lett., Vol. 27, No. 11, pg. 634, Dec. 1975.

27. K. Lee and N. Heiman, "Magnetization in rare-earth transition metal amorphous alloy films", 20th Conf. on Magnetism and Magnetic Materials, San Francisco, Calif., Dec. 1974.

28. G. S. Cargill III, "Short-range ordering in amorphous $GdFe_2$," 19th Conf. on Magnetism and Magnetic Materials, Boston Mass., Nov. 1973.

29. R. C. Taylor, "Magnetic properties of amorphous Gd-Fe films prepared by evaporation," J. A. P., Vol. 47, No. 3, pg. 1164, March 1976.

30. Corey Metals, Stocklist and Reference Book (undated).

31. Corning Product Information Sheet on 0211 Microsheet glass, issued Jan 4, 1971 from Corning Glass works, Electronics Materials Dept., Corning, New York 14830

32. R. W. Shaw, D. E. Hill, R. M. Sandfort and J. W. Moody, "Determination of magnetic bubble film parameters from strip period domain measurements", J. A. P., Vol. 44, No. 5, pp. 2346-2349, May 1973.

33. J. A. Cape and G. W. Lehman, "Magnetic domain structures in thin uniaxial plates with perpendicular easy axis", J. A. P., Vol. 42, No. 13, pp. 5732-5756, December 1971.

34. A. Hubert, A. P. Malozemoff and J. C. Deluca, "Effect of cubic, tilted uniaxial, and orthorhombic anisotropies on homogeneous nucleation in a garnet bubble film", J. A. P., Vol. 45, No. 8, pp. 3562-3571, Aug. 1971.

35. R. F. Soohoo and K. Lee, "Transverse magnetization curves in bubble films with parameter dispersions", 20th Conf. on Magnetism and Magnetic Materials, San Francisco, California, Dec. 1974.

36. P. W. Shumate, Jr., D. H. Smith, F. B. Hagedorn, "The temperature dependence of the anisotropy field and coercivity in epitaxial films of mixed rare-earth iron garnets", J. A. P., Vol. 44, No. 1, pp. 449-454, Jan. 1973.

37. M. W. Muller, "Distribution of magnetization in a ferromagnet", Phys. Rev., Vol. 122, No. 5, PP. 1485-1489, June 1, 1961.

38. C. N. J. Wagner, N. Heiman, T. C. Huang, A. Onton and W. Parrish, "The structure of Co-Gd amorphous alloy films", 21st Conf. on Magnetism and Magnetic Materials, Philadelphia, Pa., Dec. 1975.

39. L. J. Tao, R. J. Gambino, S. Kirkpatrick, J. J. Cuomo and H. Lilienthal, "Magnetic properties of amorphous GdCo", 19th Conf. on Magnetism and Magnetic Materials, Boston, Mass., Nov. 1973.

40. A. A. Thiele, "Theory of the static stability of cylindrical domains in uniaxial platelets" J. A. P., Vol. 41, No. 3, pp. 1139-1145, Mar. 1, 1970.

41. T. Iwata, R. J. Prosen, B. E. Gran, "Perpendicular anisotropy in polycrystalline NiFe thin films", J. A. P., Vol. 37, No. 3, pp. 1285-1286, March 1, 1966.

42. R. Zwingman, "Investigation into the properties of evaporated Gd-Co films", M. S. Thesis, Rice University, May 1974.

43. T. Miyazaki and H. Hoffmann, "Magnetic anisotropy of evaporated Gd-Co films", 7th International Conf. on Magnetic Films, University of Regensburg, Germany, April 1975.

44. R. Glang, R. A. Holmwood, and R. L. Rosenfeld, "Determination of stress in films of single crystalline silicon substrates", Rev. of Sci. Inst., Vol. 36, No. 1, pp. 7-10, Jan. 1965.

45. R. W. Hoffman, R. D. Daniels, and E. C. Crittenden, Jr., Proc. Phys. Soc., B67, Pg. 479, 1954.

46. R. Glang, R. A. Holmwood and P. C. Furois, Transactions of the 3rd International Vacuum Conf., 2(III), pg. 643, 1965.

47. A. Ogawa, T. Katayama, M. Hirono, T. Tsushima, "Reversal of Hall effect and Kerr rotation in ferrimagnetic rare earth-cobalt system", 20th Conf. on Magnetism and Magnetic Materials, San Francisco, Calif., Dec. 1974.

48. D. Givord, F. Givord and R. Lemaire, "Magnetic properties of iron compounds with Yttrium, Lutetium and Gadolinium", Journal de Physique. Paris, C1, pg. 668, Feb.-March 1971.

49. K. N. R. Taylor, "Intermetallic rare-earth compounds", Adv. Phys., 20, pg. 552, Sept. 1971.

50. R. Hasegawa, "Temperature and compositional dependence of magnetic bubble properties of amorphous Gd-Co-Mo films", J. A. P., Vol. 46, No. 12, pg. 5263, Dec. 1975.

51. J. T. Carlo, D. C. Bullock and F. G. West, "A ferrimagnetic model for the exchange constant in magnetic bubble garnets", IEEE Mag. Trans., Vol. Mag. 10, No. 3, pp. 626-629, Sept. 1974.

52. R. Hasegawa, R. J. Gambino and R. Ruf, "Magnetic properties of amorphous Gd-Co-Au films", App. Phys. Lett., Vol. 27, No. 9, pg. 512, Nov. 1, 1975.

GENERAL REFERENCES:

G1. S. Chikazumi, Physics of Magnetism, J. Wiley and Sons, Inc., 1959.

G2. L. I. Maissel and R. Glang, Handbook of thin film technology, McGraw-Hill Book Company, 1970.

G3. A. H. Bobeck and E. Della Torre, Magnetic Bubbles, edited by E. P. Wohlfarth, Amsterdam, The Netherlands; North Holland, 1975.

APPENDIX: Magnetization calculation program

The magnetization of a sublattice by the mean molecular field theory is:

$$M_i = n_i m_i$$

$$M_i = n_i g_i u_b \bar{S}_i$$

$$M_i = n_i g_i u_b S_i B_{j_i}(X_i)$$

$$M_i = n_i g_i u_b S_i B_{j_i}(g_i u_b S_i H_i / kT)$$

where n_i is the number of atoms/cc of type i

m_i is the number of moments/atom of type i at temperature T

g_i is the gyromagnetic ratio of atoms of type i

u_b is the Bohr magneton

S_i is the spin/atom of type i at 0 K

H_i is the mean molecular field acting on a spin of type i

$\bar{S}_i$ is the spin /atom of type i at temperature T

X is the argument of the Brillouin function

The molecular fields for a two sublattice model are:

$$\begin{bmatrix} H_1 \\ H_2 \end{bmatrix} = \begin{bmatrix} \lambda_{11} & \lambda_{12} \\ \lambda_{21} & \lambda_{22} \end{bmatrix} \times \begin{bmatrix} M_1 \\ M_2 \end{bmatrix}$$

where λ_{ij} is the molecular field coefficient between the j^{th} sublattice and the i^{th} molecular field. For a two sublattice ferrimagnetic the saturation magnetization is $M_s = |M_1 - M_2|$. The molecular field coefficients, λ_{ij}, can be related to the exchange integrals, J_{ij}, by

$$\lambda_{ij} = 2J_{ij}z_{ij}/n_j g_i g_j u_b^2$$

where z_{ij} is the corresponding i-j coordination number,

Amorphous considerations: After Hasegawa [52]. In an amorphous ferrimagnet there are no sublattices because only short range ordering exists. But, for discussion purposes the term "sublattice" will be retained. Also, the nearest neighbor positions are assumed random. By assuming a random distribution of atoms over the amorphous atomic sites with an average coordination number of 12, for a material $(A_xB_{1-x})_{1-y}C_y$ the number of nearest neighbors z_{ij} are:

$$z_{11}=12(1-y)x=z_{21}$$
$$z_{22}=12(1-y)(1-x)=z_{12}$$

For $(Fe_xGd_{1-x})_{1-y}A_y$ calculations $J_{21}=J_{12}$, $g_i=g_j=2$ and $S_{gd}=3.5$ are assumed. Also the density is assumed to be linear with atomic fraction [39].

$$\rho_{xyz}=\rho_x\cdot x+\rho_y\cdot y+\rho_z\cdot z \qquad \text{where } x+y+z=1$$

And using the conversion of atomic fraction to weight fraction

$$\rho_xK_x/\rho_{xyz}=x\cdot AtWt_x/(x\cdot AtWt_x+y\cdot AtWt_y+z\cdot AtWt_z)$$

where K_i is the ratio of i type atoms/cc in the film to i type atoms/cc in pure bulk. The number of atoms/cc of i type in the film can be found from

$$n_i=K_iA_v\rho_i/AtWt_i \qquad A_v \text{ is Avagadro's number}$$

Using the above equations a program was written for a Tektronix 31 desk calculator which would solve the simultaneous sublattice magnetization equations. The flow chart and variable definations for this program are presented here.

Variable list:

X_o	starting composition value
J_{ij}	exchange integrals
u_{fe}	iron moment
x,y,z	atomic fractions of $Gd_zFe_xA_y$
u_b	Bohr magneton
LBL F	name of subrouting F; calculates density, atomic densities and molecular field coefficients
LBL B	name of subroutine B; calculates Brillouin function
LBL S	name of subroutine S; calculates magnetization
S	spin value
M_{old}	old sublattice magnetization value
M_{new}	calculated new magnetization value
X_{fe},X_{gd}	arguments of Brillouin functions
J_{fe},J_{gd}	order of Brillouin functions
$B_J(X)$	Brillouin function
M_{fe}, M_{gd}	iron and gadolinium sublattice magnetizations respectively
ΔM_{fe},ΔM_{gd}	change in sublattice magnetizations due to recalculation
ρ_{xyz}	alloy density
K_x,K_y,K_z	ratios of atomic densities in alloy to atomic densities in bulk
λ_{ij}	molecular field coefficients.

MAIN PROGRAM

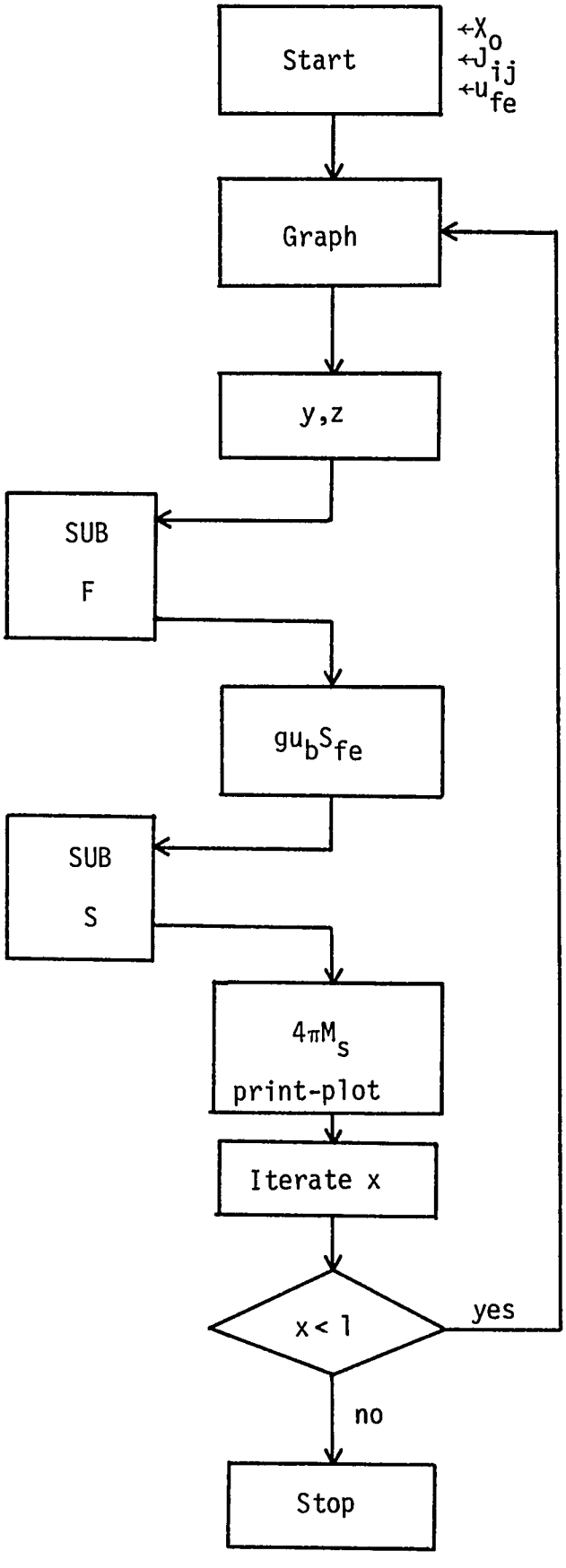

SUB S

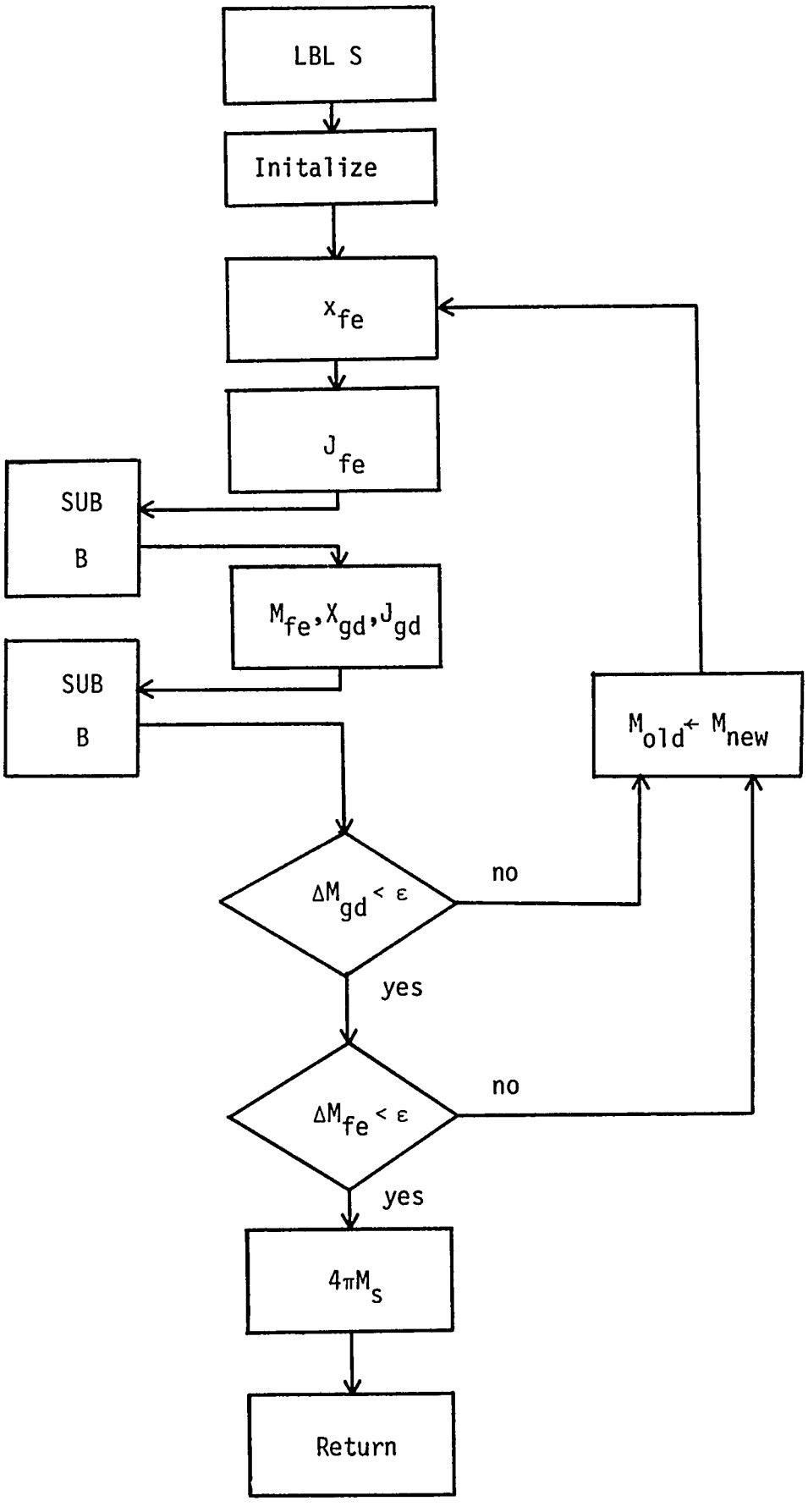
LBL S
Initalize
x_{fe}
J_{fe}
SUB B
M_{fe}, X_{gd}, J_{gd}
SUB B
$M_{old} \leftarrow M_{new}$
$\Delta M_{gd} < \varepsilon$
no
yes
$\Delta M_{fe} < \varepsilon$
no
yes
$4\pi M_s$
Return

SUB F

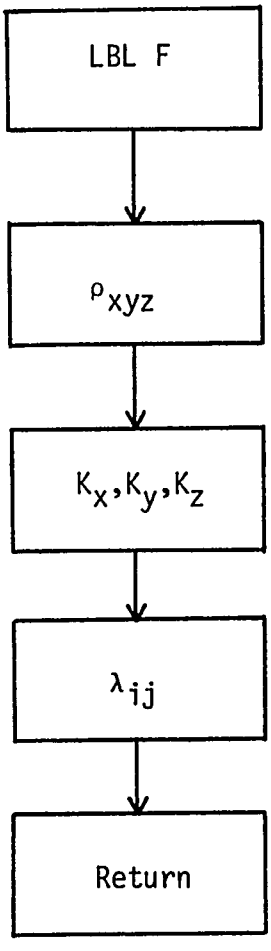

SUB B

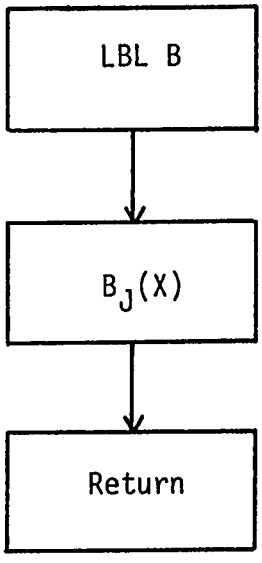

APPENDIX: Strain estimation

Consider an unstressed circular film of area A and radius r. It is then subjected to an isotropic in-plane stress σ by being adhered to a substrate. The film area is $A+\Delta A$ and the radius is $r+\Delta r$. The fractional change in the area is about

$$\Delta A/A \simeq 2\Delta r/r \simeq 2e$$

If a film which is detached from the substrate such that it is dome-shaped, see figure A-1, the height and radius are designated δ and r respectively. The surface area of the domed film is $\pi(\delta^2+r^2)$. If this domed surface is forced to occupy the area of its base πr^2, the change in its area is $-\pi\delta^2$ and the fractional change in its surface area is $-\delta^2/r^2$.

The assumption is made that the area of a detached film, which is domed shape, is unstressed. This assumption is not completely valid because the edges of the film that are detached are under compression due to the pinning effects of the substrate. However, the assumption is made to give a rough estimate of the film strain. The film strain is about $e=-(1/2)\delta^2/r^2$.

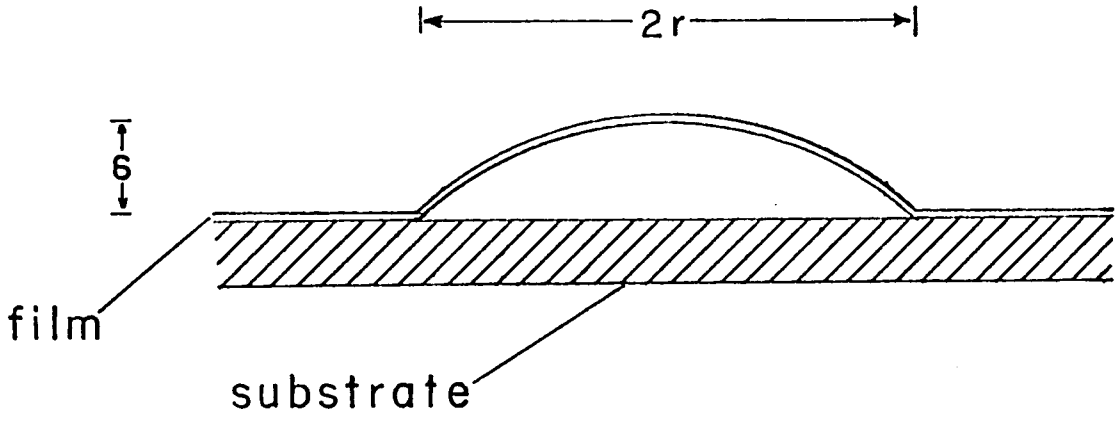

Figure A-1: Illustration of the strain estimation technique. The strain is about $-(1/2)\delta^2/r^2$.